https://doi.org/10.5194/egusphere-2025-3329
Preprint. Discussion started: 17 July 2025

NO_x emissions changes from 2019 to 2021 in Eastern China as estimated through variational inversions and TROPOMI satellite data

Rimal Abeed[1], Audrey Fortems-Cheiney[2], Grégoire Broquet[1], Robin Plauchu[1], Isabelle Pison[1], Antoine Berchet[1], Elise Potier[2], Bo Zheng[3], Gaëlle Dufour[4], Adriana Coman[5], Dilek Savas[4], Guillaume Siour[5], Henk Eskes[6], Beatriz Revilla-Romero[7], Antony Delavois[8], and Philippe Ciais[1]

[1]Laboratoire des Sciences du Climat et de l'Environnement, CEA-CNRS-UVSQ, Gif-sur-Yvette, France
[2]Science Partners, Quai de Jemmapes, 75010 Paris, France
[3]Shenzhen Key Laboratory of Ecological Remediation and Carbon Sequestration, Institute of Environment and Ecology, Tsinghua Shenzhen International Graduate School, Tsinghua University, Shenzhen, 518055, China
[4]Université Paris Cité and Univ Paris Est Créteil, CNRS, LISA, F-75013 Paris, France
[5]Univ Paris Est Créteil and Université Paris Cité, CNRS, LISA, F-94010 Créteil, France
[6]Royal Netherlands Meteorological Institute (KNMI), De Bilt, the Netherlands
[7]GMV, Remote Sensing and Geospatial Analytics Division, Madrid, Spain
[8]European Space Agency (ESA), Rome, Italy

Correspondence to: Rimal Abeed rimal.abeed@lsce.ipsl.fr

Abstract

China is one of the largest emitters of nitrogen oxides NO_x (= NO + NO_2) globally. With ongoing efforts and global pressure to reduce its emissions, up-to-date estimates of NO_x emissions remain essential. In this study we focus on the evolution of NO_x emissions over Eastern China (101.75-132.25°E; 17.75-50.25°N) between 2019 and 2021, including the analysis of the impact of the COVID-19 outbreak and the Chinese Lunar New Year national break (LNY) on NO_x emissions. We exploit the high spatial resolution and coverage of the TROPOMI Sentinel-5 Precursor nitrogen dioxide (NO_2) observations, and provide an estimate of this evolution down to the level of Chinese provinces. We assimilate TROPOMI NO_2 observations in NO_x atmospheric inversions based on the variational inversion drivers of the Community Inversion Framework (CIF), coupled to a 0.5° resolution configuration of the CHIMERE regional chemistry transport model.

Our results show a decrease in NO_x anthropogenic emissions in most of Eastern China during early 2020 compared to 2019. This decrease approaches −40% in February 2020 as compared to 2019 due to i) the lockdowns and strict regulations on mobility associated with the COVID-19 outbreak (lockdowns extended from 23 January to 8 April in Wuhan, and from late January or early February 2020 in other parts of China, extending till March 2020) and ii) the celebrations of the LNY that took place during February 2020, before the lockdowns were imposed. In some Chinese provinces, such as Shanghai, Qinghai, Jiangsu, Hubei, Henan and Beijing, the reductions in NO_x emissions were −38%, −29%, −31%, −36%, −24%, and −16% respectively during February 2020 relative to 2019. The annual total (anthropogenic + biogenic) emissions of NO_x in Eastern China decreased by −0.2 $TgNO_2$/year in 2020, compared to 2019. However, in 2021, our estimates show an annual increase of +4% in NO_x emissions as compared to 2019, amounting to 16.7 $TgNO_2$/year in 2021.

This study advances emissions quantification by delivering NO_x emissions down to the scale of Chinese provinces, a refinement that is not always addressed in regional inversions. Our approach, therefore, makes it possible to evaluate targeted policy interventions by resolving sub-national

https://doi.org/10.5194/egusphere-2025-3329
Preprint. Discussion started: 17 July 2025

emissions. This shows how crucial it is to use high-resolution data when working to improve air quality and address climate change.

1. Introduction

Besides being one of the most populated countries (1.4 Billion inhabitants in 2019 according to the Chinese census data (NBSC, 2023)), China's exports are the highest globally ($2.75T vs. $1.52T in the United States (U.S.) that comes next (OEC, 2022); China is the leading manufacturing country as it accounted for 29% out of the global manufacturing output during 2023 (China Power Team, 2024). Such industrial activities are directly linked to high levels of energy consumption and fossil fuel use (Abdelwahab et al., 2024). Since 2005, China has also been considered the main emitter of nitrogen oxides (NO_x= NO + NO_2) in the world, followed by the U.S. and then the European Union (Wang et al., 2022). NO_x emissions are mainly driven by fossil fuel combustion, for instance due to transportation (Zheng et al., 2018a), power plants (Tang et al., 2020), and some types of industrial processes (e.g. steel, iron and cement productions among others) (Bo et al., 2021; J. Liu et al., 2021).

NO_x are air pollutants that are crucial to tropospheric chemistry. For instance, the photo-oxidation of NO_x is a major source of nitrous acid (HONO), the latter accelerates the formation of tropospheric ozone (O_3) (Song et al., 2023). O_3, when in the troposphere, is damaging to human health (Donzelli & Suarez-Varela, 2024) and to the ecosystem (Agathokleous et al., 2020). NO_x gases act as oxidizing agents and therefore intervene in the chemistry of volatile organic compounds (VOCs) (Atkinson, 2000), these gases have been linked to a variety of physical diseases (Soni et al., 2018). Due to their role in particulate matter (PM) formation and particle growth, NO_x gases were found to be linked to haze episodes in China (H. He et al., 2014). In addition to their impact on the environment, NO_x emissions are one of the drivers of the increase of premature death due to deteriorated air quality, with numbers of deaths that are expected to be higher in the future (Bressler, 2021). In a study carried out in the Netherlands, Zock et al. (2018) found a positive link between air pollution and diseases such as asthma, diabetes, headaches, among others; they included in their analysis pollution by PM ($PM_{2.5}$ <2.5 μm, and PM_{10} <10 μm) and NO_2 gas. The exposure to high amounts of NO_x gases increases the risk of mental health disorders (e.g., anxiety, depression, and even suicide attempts), as Shaw and Van Heyst (2022) showed a positive correlation between the risk ratio -referring to the increased risk linked to an increase of NO_2 concentration by 10 $\mu g \cdot m^{-3}$- and the exposure rate of NO_2. Ju et al. (2023) have also demonstrated the impact of NO_x-related air pollutants (O_3 and $PM_{2.5}$) on mental health in highly polluted cities over China.

In 2006, the Chinese government put in place the 11th 5-year plan (2006 – 2010) (NPC, 2006) to control air pollutants such as sulfur dioxide (SO_2) and PM. In 2011, NO_x control was added to the 12th 5-year plan (2011 – 2015), to reduce the annual Chinese NO_x emissions by 10% compared to 2010. And later in 2018, an action plan for a duration of three years was introduced, this plan aimed at reducing the emissions of both SO_2 and NO_x emissions gases by a minimum 15% as compared to 2015 (S. Li et al., 2023). Chinese policies seem to succeed in reducing the NO_x emissions and therefore the NO_2 concentrations after 2010 (Ding et al., 2017), and remarkably, the gross domestic product (GDP) started decoupling from the NO_x emissions in 2011 (S. Li et al., 2023). Nevertheless, the decrease in NO_2 concentrations did not necessarily lead to an equivalent enhancement in air quality. Some studies argued that the alteration in the balance of the VOC/NO_x ratio did in fact lead to an increase in surface

https://doi.org/10.5194/egusphere-2025-3329
Preprint. Discussion started: 17 July 2025

O_3 concentrations (R. Li et al., 2024; Lu et al., 2023) causing haze episodes in Shanghai (Le et al., 2020). An accurate account of NO_x emissions in space and time is needed to i) assess the effectiveness of policies aimed at reducing NO_x emissions and ii) to understand the impact of the evolution of NO_x emissions and of NO_2 concentrations on air quality.

The quantification of anthropogenic NO_x emissions following a bottom-up (BU) approach, based on the statistics of activity sectors and fuel consumption and relying on emission factors per activity type, suffers from relatively large uncertainties at the national and annual scales (Ding et al., 2017) and bear, in addition to that, large spatial and temporal differences (Ding et al., 2017; Jena et al., 2015). Saikawa et al. (2017) have compared five different inventories focusing on the estimates of Chinese NO_x emissions, including the Regional Emission inventory in ASia v2.1 (REAS), the Multi-resolution Emission Inventory for China (MEIC), the Emission Database for Global Atmospheric Research v4.2 (EDGAR), the inventory by Yu Zhao (ZHAO), and the Greenhouse Gas and Air Pollution Interactions and Synergies (GAINS). They have shown that large discrepancies between the BU estimates were mainly related to different statistical data and emission factors for the energy and transport sectors, as inventories used different provincial statistics (Saikawa et al., 2017). To develop accurate, high-resolution emission inventories, integrating independent information sources is essential. Atmospheric measurements can serve as a valuable complement to current BU approaches, thereby enhancing the spatial precision of emission inventories. These improvements are crucial for effectively assessing air quality policies.

Since the 2000s, NO_2 tropospheric concentrations have been monitored around the world by space-borne instruments, such as the Global Ozone Monitoring Experiment (GOME) (Burrows et al., 1999) and GOME-2 (Munro et al., 2016; Munro et al., 2016), the SCanning Imaging Absorption spectroMeter for Atmospheric CHartographY (SCIAMACHY) (Bovensmann et al., 1999; Burrows et al., 1995) and the Ozone Monitoring Instrument (OMI) (Levelt et al., 2018). In this context, attempts have been made to develop so-called top-down (TD) methods, complementary to BU inventories, to deduce NO_x emissions from NO_2 satellite data. The OMI NO_2 tropospheric vertical column densities (TVCDs) have been exploited previously to estimate NO_x emissions in China (Gu et al., 2014; Qin et al., 2023; Savas et al., 2023). For example, Savas et al. (2023) estimated the evolution of anthropogenic NO_x emissions in 2015 and 2019 compared to 2010 over Eastern China. They have found a decrease of NO_x emissions in the southern part of Eastern China over large urbanized and industrialized locations but an increase in the northern part in 2015 and 2019 compared to 2010.

The successor of OMI, the TROPOspheric Monitoring Instrument (TROPOMI) (Veefkind et al., 2012), on board the Copernicus Sentinel-5 Precursor (S-5P) satellite launched in 2017, has brought images of NO_2 with higher spatial resolution (pixel size of about 5.6 km × 3.5 km since August 2019). With a swath as wide as approximately 2600 km on ground, TROPOMI also provides daily coverage. This higher spatial resolution increases the potential to quantify local emissions (from specific provinces, urban or industrial areas, sometimes from specific large industrial sites). It also supports improved precision in NO_x emission estimates at large scales by offering better insights into spatial heterogeneity in chemistry and emission processes (e.g., industrial vs. urban areas) at fine scales.

Both OMI and TROPOMI NO_2 observations have also been used to quantify the impact on NO_2 concentrations of the Lunar New Year national holiday (LNY), which is a 7 to 14-days of celebration with businesses and factories closed that takes place every year around late January – mid February

(Bauwens et al., 2020; Chu et al., 2021; Cooper et al., 2022; Pei et al., 2020; Tan et al., 2009). By the end of 2019, and in the middle of the 3-year action plan (2018 – 2020), the COVID-19 pandemic broke in Wuhan. The latter is one of the multiple megacities in China that hosted 11.21 million inhabitants in 2019 (HKTDC Research, 2022). As a response to the increasing rates of infections and deaths caused by the COVID-19 virus, the Chinese government implemented strict mobility regulations across various provinces starting early 2020 and extending until early April 2020 in some cases. The applied measures varied based on the number of infection cases reported (Chinazzi et al., 2020; R. Li et al., 2020). For instance, in Wuhan, a full 76-day lockdown was imposed, the longest in China, and it extended from the 23rd of January 2020 up until the 8th of April 2020 (R. Li et al., 2020). In other Chinese cities, shorter lockdown periods accompanied by lighter measures were imposed, the periods varied between 3 and 60 days. Due to the reduction in mobility and the stay-home rule imposed by the Chinese government, the NO_2 TVCDs and the NO_x emissions were expected to have significantly dropped during the period of the lockdown (Bauwens et al., 2020; Ding et al., 2020; Zhang et al., 2020; Levelt et al., 2022; H. Li et al., 2024; S. Li et al., 2023).

If all the inverse modeling studies about the COVID-19 crisis agree that NO_x emissions were indeed reduced during the lockdown period in 2020 (T.-L. He et al., 2022; Q. Zhang et al., 2020; R. Zhang et al., 2020; Wei et al., 2023; Ding et al., 2020; H. Li et al., 2024), they differ on the extent of these reductions. The simplest approaches extrapolate the relationship between the tropospheric concentrations and the emissions from a single perturbation of the emissions in the CTM simulations, and from the assumption that this relationship is purely local (occurring within the scale of the CTM grid cell) (H. Li et al., 2024; Zheng et al., 2021). These simplifications and assumptions provide a limited capability to account for the chemistry. A more detailed account of the complex NO_x chemistry with more elaborate approaches using chemistry-transport models (CTMs) with ensemble Kalman filter inverse modelling techniques or variational approaches should support more accurate derivations of NO_x emissions from NO_2 satellite data.

In this study, we leverage the high spatial resolution and extensive coverage of NO_2 tropospheric columns provided by TROPOMI instrument, onboard the Sentinel 5-Precursor satellite, to estimate NO_x emissions in Eastern China, where the Chinese NO_x emissions are the highest, at the relatively high horizontal resolution of 0.5°×0.5° for the period 2019 – 2021, that includes changes in emissions due to Chinese emissions reduction policies, lockdown measures, and LNY holidays. The relatively fine spatial resolution makes it possible to estimate the decrease/increase of NO_x emissions down to the provincial level. We therefore study the impact of COVID-19 lockdown measures, as well as the effect of the LNY on the emissions of NO_x in a total of 26 provinces over Eastern China. To estimate these emissions, we conduct variational inversions at 0.5° and 1-day resolution with the Community Inversion Framework (CIF, Berchet et al., 2021), using the CHIMERE CTM (Mailler et al., 2017; Menut et al., 2013), including a chemistry module taking into account the complex NO_x chemistry in gas-phase, its non-linearities, and its adjoint (Fortems-Cheiney et al., 2021). This framework and the regional inversion configuration are built upon the work done by Fortems-Cheiney et al. (2021, 2024), Savas et al. (2023) and Plauchu et al. (2024). **Section 2** presents the data sources and pre-processing, as well as the regional inverse modelling configuration. **Section 3** presents the results and discusses them, and the last section summarizes the conclusions.

https://doi.org/10.5194/egusphere-2025-3329
Preprint. Discussion started: 17 July 2025

2. Data and Methods

2.1. Configuration of the CHIMERE CTM for the simulation of NO_2 concentrations in Eastern China

Study domain boundaries	101.75-132.25°E; 17.75-50.25°N
Horizontal resolution	0.5°×0.5°, 61 × 65 grid cells (longitude × latitude), i.e., 3965 grid cells per level
Vertical resolution	17 layers extending from the surface up to 200 hPa (around 12 km above the sea level)
Meteorological fields	European Centre for Medium-Range Weather Forecasts (ECMWF) operational meteorological forecast (Owens and Hewson, 2018)
Initial and boundary conditions (excluding NO_x)	LMDZ-INCA (Szopa et al., 2009)
Anthropogenic emissions	A combination of Carbon-Monitor (Z. Liu et al., 2020), Community Emissions Data System (CEDS, Hoesly et al., 2019, 2018), MEIC data (Zheng et al., 2018b), and EDGAR-HTAP-v2.2 for VOCs (Janssens-Maenhout et al., 2015)
Biogenic soil emissions (NO+VOCs)	Model of Emissions of Gases and Aerosols from Nature (MEGAN) (Guenther et al., 2006)
Chemical Scheme	MELCHIOR-2 (Carter, 1990; Derognat et al., 2003)

Table 1. The configuration of CHIMERE for the simulation of NO_2 concentrations in Eastern China. See **Figure 1** for a map of the domain. MELCHIOR-2: Modèle Lagrangien de Chimie de l'Ozone à l'échelle Régionale, gas-phase chemical reaction scheme.

CHIMERE CTM is designed for the study of regional atmospheric pollution events (e.g., Ciarelli et al., 2019; Menut et al., 2020), and is part of the operational ensemble of the Copernicus Atmosphere Monitoring Service (CAMS) regional services. The long series of publications on air quality modelling with this CTM, including comparisons to observations, support the reliability and the accuracy of the CHIMERE simulations over regions such as Eastern China. In particular, C. Gao et al. (2024) showed that CHIMERE provides reliable simulations of air quality and NO_2 concentrations over this region, effectively capturing annual and seasonal spatiotemporal characteristics when evaluated against surface and satellite observations.

The configuration set for the CHIMERE simulations in this study is summarized in **Table 1**. CHIMERE is driven here by meteorological fields at a fine resolution of 0.25°, from the European Centre for Medium-Range Weather Forecasts (ECMWF) operational meteorological forecast (Owens and Hewson, 2018). The MELCHIOR-2 scheme includes 120 oxidation reactions of 40 gaseous species.

https://doi.org/10.5194/egusphere-2025-3329
Preprint. Discussion started: 17 July 2025

Figure 1. The study domain covers the Chinese provinces of mainland China, hereafter called "Eastern China". The model grid cells are shown in dashed grey.

Considering the short lifetime of NO_2, we do not consider its influx from outside the domain: its boundary conditions are set to zero, as in Savas et al. (2023), Plauchu et al. (2024) and in Fortems-Cheiney et al. (2024). Nevertheless, the lateral and top boundaries for other species, such as O_3, nitric acid (HNO_3), peroxyacetyl nitrate (PAN) and formaldehyde (HCHO), participating in the NO_x chemistry are considered, as in Savas et al. (2023), in Plauchu et al. (2024) and in Fortems-Cheiney et al. (2024). In this study, Eastern China refers to the Chinese mainland included in the study domain (**Figure 1**).

2.2. Prior estimates of NO_x emissions in Eastern China

The main goal of an inversion is to correct a-priori emission maps, that we refer to as "prior" emissions/estimates. In this study, the anthropogenic prior estimates are a combination of three inventories: the Community Emissions Data System (CEDS) (R. Hoesly et al., 2018, 2019), the Carbon Monitor (Z. Liu et al., 2020), and the Multi-resolution Emission Inventory model for Climate and air pollution research (MEIC) (Zheng et al., 2018b). The resulting prior estimates used for this study are therefore referred to as CEDS-CarbonMonitor-MEIC (CCMM). In the combination of these three inventories, CEDS provides gridded monthly emissions for the year 2019 at a 0.5°×0.5° horizontal

https://doi.org/10.5194/egusphere-2025-3329
Preprint. Discussion started: 17 July 2025

resolution; these monthly estimates are downscaled to daily emissions based on daily variations from Carbon Monitor for the period 2019 - 2021; finally, the process of temporal disaggregation from daily to hourly emissions relies on typical diurnal emission profiles by sector derived from MEIC (Zheng et al., 2018b. CEDS employs a comprehensive approach that integrates various emissions inventories, factors, and activity data to derive emission estimates at national and sectoral scales (Hoesly et al., 2018, 2019). CEDS monthly emissions are produced from aggregated estimates, leveraging spatial proxy data from the EDGAR gridded emissions dataset and distributed for nine final gridded sectors (agriculture, energy, industrial, transportation, residential and commercial, solvents production and application, waste, international shipping, and aviation). The agricultural sector includes soil emissions due to agricultural practices, derived from the EDGAR inventory (Crippa et al., 2018). Among these sectors, we exclude aviation for this study. To obtain daily emissions, Carbon Monitor daily variations for each month, sector, and region are used. These variations are derived from CO_2 daily estimates. The impact of the 2020 lockdown is therefore considered in CCMM via the relative temporal variations extracted from the Carbon Monitor (illustrated in **Figure 2** for February, shown for the other months of the year in Figures S1, S2, and S3). NO_x emissions are expressed in either teragram or kiloton in equivalent NO_2 ($TgNO_2$ or $ktNO_2$) throughout the study.

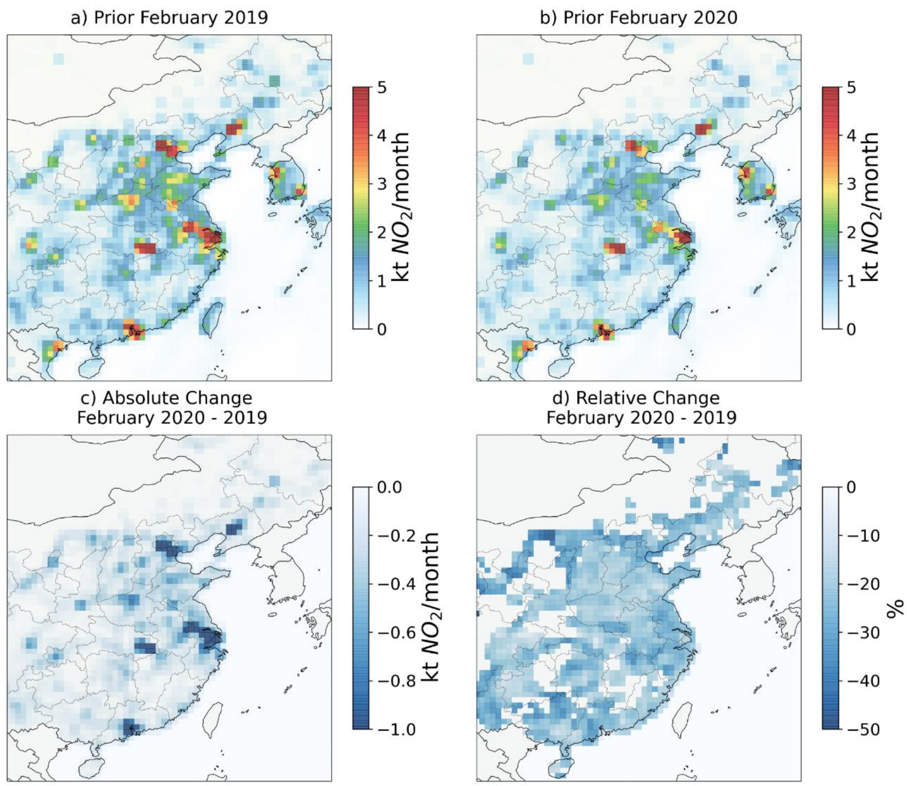

Figure 2. Prior estimates of NO_x total (anthropogenic + biogenic) emissions for February 2019 (a) and 2020 (b), and the absolute (c) and relative (d) change between these estimates. Values below 0.3 kt NO_2 in the prior estimate for February 2019 are set to zero when calculating the relative difference (d) to reduce the noise in the figure. The total relative difference across the entire domain (shown in panel d) is –22%.

https://doi.org/10.5194/egusphere-2025-3329
Preprint. Discussion started: 17 July 2025

In addition to NO_x anthropogenic emissions, NO biogenic emissions from soil microbial activity are considered. These NO biogenic soil emissions are based on simulations from the Model of Emissions of Gases and Aerosols from Nature (MEGAN) (Guenther et al., 2006), with a ~ 1 km × 1 km spatial resolution. These biogenic simulations do not provide soil emissions due to agricultural practices (these are included in the anthropogenic CCMM inventory). The lightning-generated NO_x are not taken into account in the prior estimation. In China, the lightning-produced NO_x (LNO_x) emissions are estimated at 516 to 1054 $ktNO_2.yr^{-1}$ (Q. Li et al., 2023), and they contribute up to 7.5% to the total tropospheric NO_x emissions (Fengxia et al., 2016). Fire emissions are neglected, as their contribution to the NO_x total emissions in China is relatively small 230 (50–450) $ktNO_2.yr^{-1}$ (Yin et al., 2019), which amount to approximately 1.15% of the total national NO_x emissions. All the emission data are spatially aggregated at the horizontal resolution of 0.5°×0.5° of the CHIMERE grid.

2.3. NO_2 TVCDs from TROPOMI

In this study we use NO_2 TVCDs from the TROPOMI instrument (Veefkind et al., 2012). TROPOMI is a nadir-viewing hyperspectral spectrometer that covers a large spectral range (270 – 2385 nm) from the ultraviolet (UV) to the shortwave infrared (SWIR) (Lambert et al., 2024). S-5P is following a sun-synchronous polar orbit, and has a daily overpass at 13:30 solar local time. TROPOMI has a swath of ~2600 km, with a spatial resolution of 3.5×5.5 km² (since 6 August 2019, and 3.5×7 km² prior to that time), and it covers latitudes between 7° and 7°.

We use reprocessed (RPRO) version 02.04.00 from TROPOMI NO_2 products, from January 2019 to December 2021. The main update in this version, compared to previous versions, is that it uses a spectral surface reflectivity climatology derived from TROPOMI (Tilstra et al., 2024) replacing the older OMI and GOME-2 (the Global Ozone Monitoring Experiment-2) datasets used in versions 1.0.2 to 2.3.1. This replacement, which also accounts for the directionality of the Lambertian Equivalent Reflectivity (LER), leads to significant changes in the cloud retrievals (van Geffen et al., 2022).

TROPOMI RPRO-v02.04.00 data and ground-based MAX-DOAS data, from 31 stations globally, continue to show discrepancies that vary with the level of pollution near the station (Lambert et al., 2024). However, when MAX-DOAS profile data are vertically smoothed using the S-5P averaging kernels (AKs), the bias is positive (+10%) over non-polluted areas and negative (-32%) over highly polluted areas. Furthermore, comparisons of NO_2 total columns with the Pandora direct-sun spectrometer (Herman et al., 2009), which provides robust column measurements due to its trivial light path, show a median bias of -8% overall, with a positive bias of 4% at clean, high-altitude sites and a negative bias of -15% in polluted areas (Lambert et al., 2025). These biases are reduced when AKs are used, as in this study. We select data with a quality assurance (QA) value of 0.75, following the criteria of Lambert et al. (2024, 2025).

https://doi.org/10.5194/egusphere-2025-3329
Preprint. Discussion started: 17 July 2025

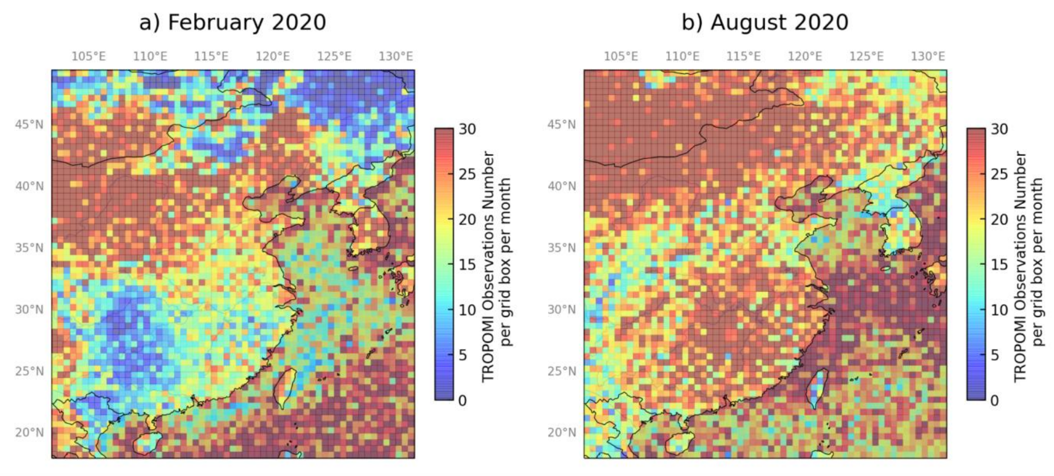

Figure 3. Number of TROPOMI observations (with a quality flag qa > 0.75) of tropospheric NO_2 (cloud-free) per 0.5° resolution grid-cell, during a winter month (a) and a summer month(b) in 2020.

In winter, some areas have a relatively lower observation number, as compared to the rest of the domain and to summer months (**Figure 3**). This is mainly due to the larger cloud cover, but other factors have an impact, such as the solar zenith angle, aerosol optical thickness and surface albedo (M. Gao et al., 2023). Overall, TROPOMI provides reliable and consistent coverage of the studied domain, during both summer and winter, which makes it possible to estimate emissions down to the provincial level.

2.4. Consistent comparison between simulated and observed NO_2 TVCDs

In order to compare NO_2 TVCDs simulated by CHIMERE with those provided by TROPOMI observations, we need to tackle several differences between the satellite instrument and the CTM 3D simulated NO_2 concentration fields. For example, these differences include: 1) spatial and temporal resolutions, and 2) variations of the instrument retrieval sensitivity to the concentrations along the vertical columns characterized by the retrieval AKs. A "super-observation" approach (Eskes et al., 2003; Miyazaki et al., 2012) is employed to aggregate the observations and derive errors (uncertainties from the retrieval process, including the propagation of the instrumental noise) and vertical sensitivity at the model resolution (Fortems-Cheiney et al., 2021; Plauchu et al., 2024; Savas et al., 2023). The temporal resolution is addressed, by matching the overpass of the S-5P satellite to the time stamps in the simulated TVCDs from CHIMERE. At a given time, in each model grid-cell covered by TROPOMI observations, the super-observation is defined as the observation (TVCD, errors and AKs) corresponding to the TVCD value closest to the mean of all the observations within this 0.5°×0.5° grid cell, and within the corresponding CHIMERE physical time step of approximately 5 to 10 minutes, following the method described by Plauchu et al. (2024). The super-observation errors were assigned as in Plauchu et al. (2024), so as to account for spatially correlated systematic uncertainties in TROPOMI NO_2 retrievals.

https://doi.org/10.5194/egusphere-2025-3329
Preprint. Discussion started: 17 July 2025

The simulated NO_2 TVCDs (**Figure 4**a, d for two months) broadly capture the spatial and temporal variabilities of those provided by TROPOMI (**Figure 4**c, f).

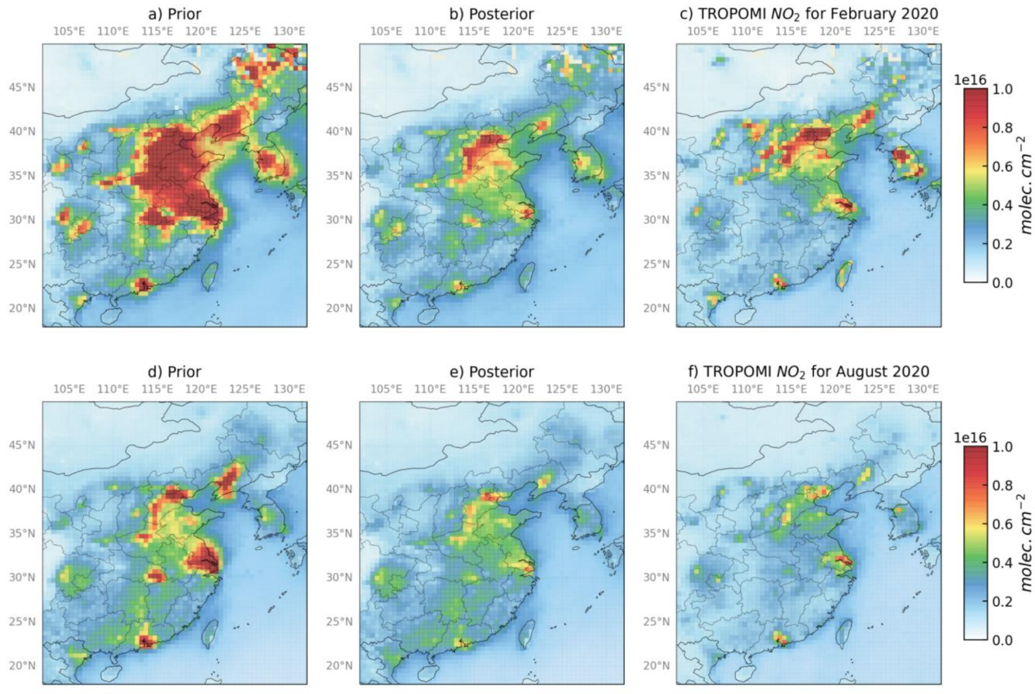

Figure 4. Monthly means of the NO_2 TVCDs corresponding to the TROPOMI super-observations at 0.5° resolution during February (upper row) and August (bottom row) 2020. The CHIMERE prior TVCDs are shown in the first column (a, d), the posterior estimates using the correction of the prior are shown in the second column (b, e), and the TVCDs from TROPOMI are shown in the last column (c, f).

2.5. Variational inversion of NO_x anthropogenic and biogenic soil emissions

The NO_x emission estimates from the inversion (called "posterior" estimate of the emissions) consist in a correction of the prior estimates of NO_x emissions (described in **Section 2.2**), which reduce the differences between the simulated NO_2 and the TROPOMI NO_2 super-observations. We use a Bayesian variational inversion framework, similar to the one used in Fortems-Cheiney et al. (2021, 2024), Savas et al. (2023) and Plauchu et al. (2024). To cover the period from 2019 to 2021, we conduct a series of monthly inversions (covering 1-month windows) that are later combined; each inversion is independent of the others. In each iteration, the posterior emissions, are derived from the minimization of the cost function $J(x)$, stated below as **Equation 1**:

$$J(x) = ½\left(x - x^b\right)^T B^{-1}\left(x - x^b\right) + (H(x) - y)^T R^{-1}(H(x) - y) \qquad \textit{Equation 1}$$

The control vector $\boldsymbol{x}$, contains variables that are corrected by the inversion, which, here, all underlay the estimates of the surface emissions of NO and NO_2 in input of CHIMERE, while $\boldsymbol{x}^{\boldsymbol{b}}$ is the prior estimates of the control vector. $\boldsymbol{y}$ combines the TROPOMI super-observations. $\boldsymbol{H}$, the observation operator, links the variables in the control vector (log-space) to the observation space defined by the TROPOMI super-observations. It includes: the exponential operator and scaling of the prior emission maps that convert the maps of the logarithm of the coefficient for the emission) into emission maps at the spatial and temporal resolutions of CHIMERE; the atmospheric chemistry and transport model CHIMERE itself; and the extraction of the TVCDs from CHIMERE when TROPOMI super-observations are available (spatially and temporally).

$\boldsymbol{B}$ is the prior error covariance matrix: it fully characterizes the uncertainty in $\boldsymbol{x}^{\boldsymbol{b}}$, called prior uncertainty under the assumption that it follows an unbiased and normal distribution N(O,**B**) ; $\boldsymbol{R}$ is the observation error covariance matrix: it corresponds to the sum of uncertainties from the observation operator and from the super-observations; assuming that these errors have an unbiased and normal distribution, N(0,$\boldsymbol{R}$), they are fully characterized by $\boldsymbol{R}$.

Here, $\boldsymbol{x}$ is built so that the uncertainties in the prior estimates of the emissions are implicitly modelled assuming that they have a log-normal distribution, in order to reflect the uncertainty in the order of magnitude of these emissions and forcing the analyzed emissions to be positive (Plauchu et al., 2024). $\boldsymbol{x}$ is thus composed of logarithms of scaling coefficients to be applied to the prior estimate of the emissions.

$\boldsymbol{x}$ is split according to the anthropogenic and biogenic components of the NO and NO_2 emissions in each of the model grid cells at 0.5° resolution for each day. The information provided by the TROPOMI observations, together with the spatial and temporal resolutions of CHIMERE, do not support an accurate separation of the total NO_x emissions between NO and NO_2 emissions. However, the control vector $\boldsymbol{x}$ maintains this separation for technical simplicity, as this approach does not adversely impact the estimation of the total NO_x emissions. There is no further sectorization of the control of anthropogenic emissions. More specifically, $\boldsymbol{x}$ contains:

- the logarithms of the scaling coefficients for NO anthropogenic emissions, at a 1-day temporal resolution, and a 0.5°×0.5° (longitude, latitude) horizontal resolution; and over the 17 vertical layers of CHIMERE i.e, for each of the corresponding 61×65×17 grid cells,
- the logarithms of the scaling coefficients for NO_2 anthropogenic emissions, at the same vertical, temporal, horizontal resolutions as for NO,
- the logarithms of the scaling coefficients for NO biogenic soil emissions at a 1-day temporal resolution, and a 0.5°×0.5° (longitude, latitude) horizontal resolution at the surface (1 vertical layer), i.e. for each of the corresponding 61×65×1 grid cells.

Accordingly, $\boldsymbol{B}$, is a 3-block diagonal matrix: the first block corresponds to the logarithms of the NO anthropogenic emissions, in which each diagonal element is set at $(0.35)^2$, this variance value in the log-space corresponds to a factor ranging between 70 to 140% in the emission space, at the 1-day and model's grid scale. Similarly, the second block corresponds to the logarithms of the NO_2 anthropogenic emissions, in which each diagonal element is set at $(0.35)^2$, this variance value in the log-space corresponds to a factor ranging between 70 to 140% in the emission space, at the 1-day and model's grid scale.

https://doi.org/10.5194/egusphere-2025-3329
Preprint. Discussion started: 17 July 2025

The third block of $\boldsymbol{B}$ is set for NO biogenic soil emissions, in which each diagonal element is set at $(0.5)^2$, corresponding to a factor ranging between 60 to 164% in the emission space at the 1-day and model's grid scale.

We account for spatial correlations in the uncertainties both for anthropogenic and biogenic parts. Spatial correlations are described by exponentially decaying functions with an e-folding length of 50 km over land and over the sea as in Fortems-Cheiney et al. (2024). However, we do not account for temporal correlations between different days.

The uncertainties on the observations y and on the observation operator $\boldsymbol{H}$ are characterized by the so-called observation error covariance matrix $\boldsymbol{R}$, set up here as a diagonal matrix based on the assumption that these errors are not correlated in space or time when aggregated at the model 0.5° and 1 h resolution. The variance in the observation errors corresponding to individual observations in the diagonal of $\boldsymbol{R}$ is the quadratic sum of the error we have assigned to the TROPOMI super-observations and of an estimate of the errors from the observation operator. We assume that the observation operator error is dominated by the chemistry-transport modelling errors and -in case when the model grid-cell is covered by few TROPOMI observations- by the errors associated with the discrepancies between the spatial representativeness of the super-observations and of the model corresponding column. It is set at 20 % of the retrieval value for each super-observation, as in Fortems-Cheiney et al. (2021, 2024).

The inversion system searches for the minimum of the cost function $\boldsymbol{J}$ using the iterative M1QN3 limited-memory quasi-Newton minimization algorithm (Gilbert & Lemaréchal, 1989). At each iteration, the computation of the gradient of $\boldsymbol{J}$ relies on the adjoint of CHIMERE, which is the adjoint of the observation operator. We impose a reduction of the norm of the gradient of $\boldsymbol{J}$ by 95% as a constraint for the interruption of the minimization process.

3. Results

3.1. Improving the fit between CHIMERE simulations and TROPOMI super-observations

Before analyzing the results in terms of NO_x emissions, we check the behavior of the inversion by comparing the performance of the prior and posterior simulations in reproducing the spatial and temporal variations of the observations. We analyses the months of February and August 2020 to illustrate the typical behavior of the inversions in winter and summer, but the analysis is performed on all the months for the years 2019, 2020 and 2021 (Figures S4, S5, and S6).

TROPOMI super-observations and the corresponding CHIMERE NO_2 TVCDs present similar spatial patterns, with hotspots over Shanghai, Beijing, Wuhan, and Hong Kong, as well as in the north-eastern province, Liaoning (**Figure 4**). However, the prior simulation overestimates the NO_2 TVCDs in Eastern China compared to the observations, with a mean bias of about +30% and +12%, for February and August 2020 respectively.

https://doi.org/10.5194/egusphere-2025-3329
Preprint. Discussion started: 17 July 2025

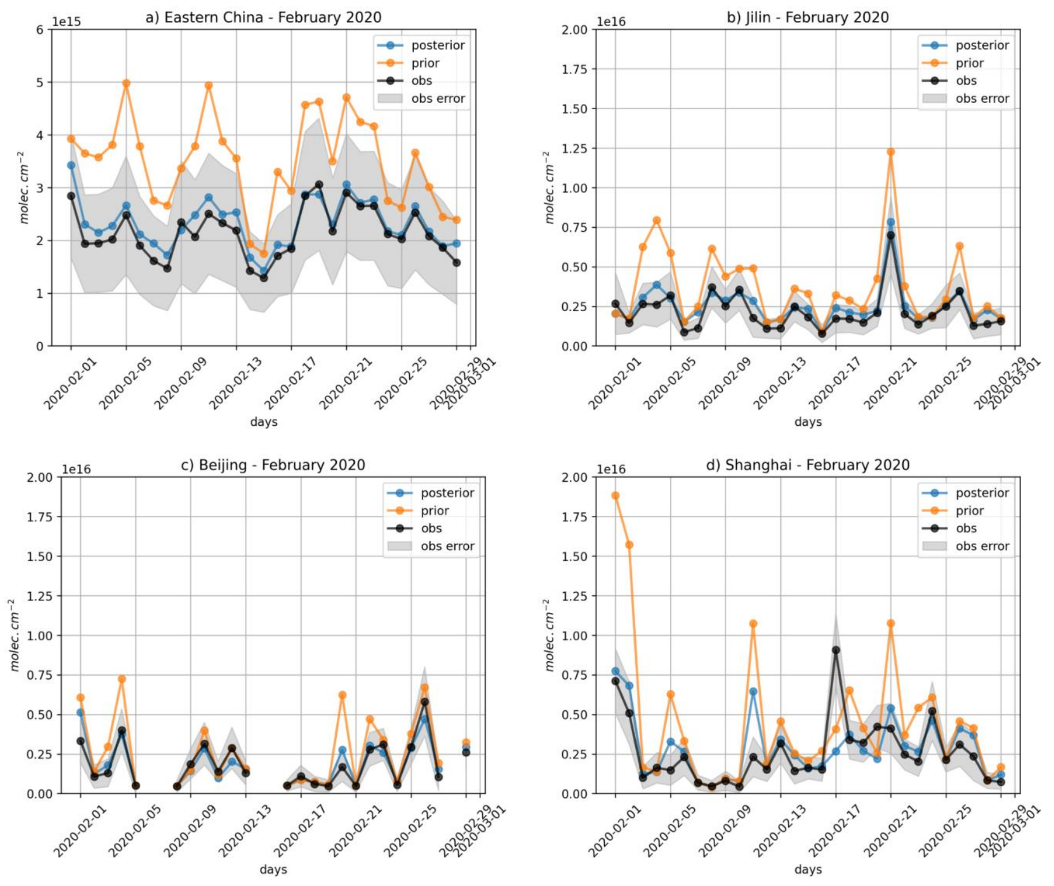

Figure 5. Daily mean posterior (blue) and prior (orange) estimations of NO_2 TVCDs as compared to that of the TROPOMI super-observations (obs, black) during February 2020, with the 1-sigma error associated to the super-observations as a grey shaded area (obs error). The top row features averages for Eastern China (a) and the province of Jilin (b), and the bottom row shows averages for the provinces of Beijing (c) and Shanghai (d). The NO2 TVCDs are expressed in molecules.cm-2. Note that the y axis limits are different for the provinces as compared to Eastern China. The provinces are shown in Figure 1 on the map of the domain.

The inversion brings the simulated NO_2 TVCDs closer to the TROPOMI super-observations (**Figure 4**; see also the time series of daily mean TVCDs in **Figure 5**). The improvement of the fit between the simulated and the observed NO_2 differs among polluted and rural regions, for instance, it is the best over polluted regions such as Shanghai, Beijing, Wuhan, Hong Kong, and Liaoning (**Figure 4**). Nevertheless, the posterior simulation still presents positive biases compared to the observations (**Figure 4** and **Figure 5**). This is partly due to 1) the limitations in the spatial and temporal coverage of TROPOMI, particularly in winter (**Figure 3**), 2) the errors associated with TROPOMI super-observations and with the CTM (assigned in the ***R*** matrix, **Section 2.5**), and 3) the potential lack of sensitivity of NO_2 TVCDs to NO_x emissions depending on the chemical regime. As the CHIMERE

https://doi.org/10.5194/egusphere-2025-3329
Preprint. Discussion started: 17 July 2025

prior simulation overestimates the NO_2 TVCDs, the inversion brings the CHIMERE NO_2 columns closer to the TROPOMI data by reducing NO_x emissions (**Figure 6, Section 3.2**).

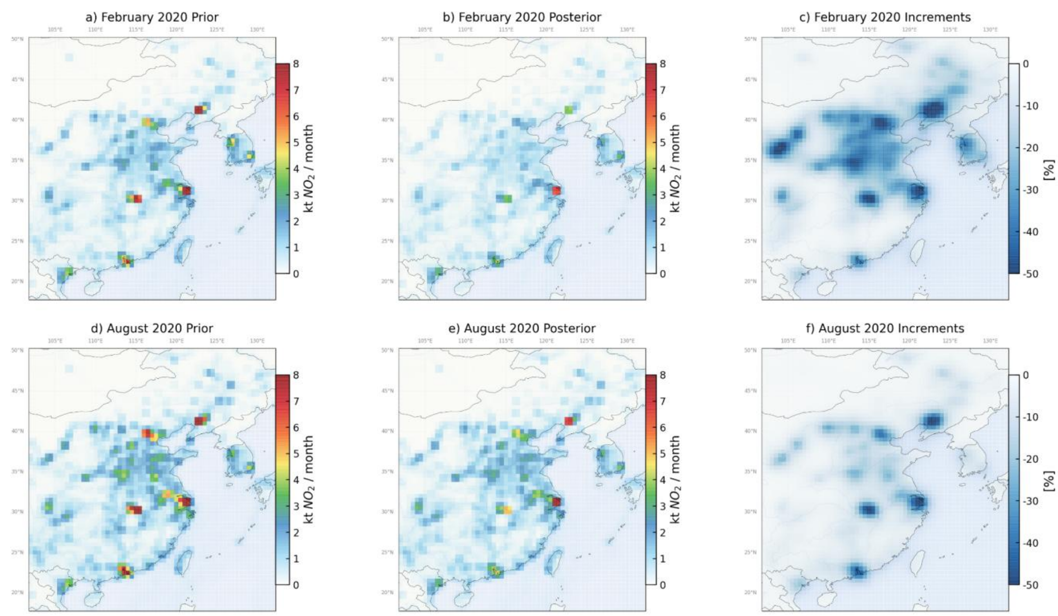

Figure 6. NO_x emissions during the months of February (top, a to c) and August (bottom, d to f) 2020. The prior (a, d) and the posterior (b, e) estimates are expressed in kilotons equivalent NO_2 ($ktNO_2$/month), and the relative increments (c, f) to the prior emissions from the inversion, in %.

3.2. NO_x annual budgets in Eastern China from 2019 to 2021

This section focuses on comparing the total (biogenic + anthropogenic) posterior NO_x emission estimates and the prior ones. NO_x posterior total emissions over Eastern China were reduced by −18% (±0.4%) compared to the prior inventory, for all years considered here (**Figure 7**). This result may be partly due to the artificial propagation of errors from the TROPOMI observations (Lambert et al., 2024; **Section 2.3**) and from the CTM. Nevertheless, the potential biases of the TROPOMI observations are considered in the characterization of our **R** matrix (**Section 2.5**). In addition, CHIMERE has been shown to be reliable for simulating air quality over Eastern China (C. Gao et al., 2024) and no large-scale modeling bias has been identified in the CHIMERE simulation of NO_2 concentrations. Our results therefore suggest that NO_x emissions are overestimated by inventories.

The increase of NOx emissions between 2019 and 2021 -which is probably linked to the evolution of the total consumption of fossil fuels in China (including coal, oil, and natural gas)- is the same in the posterior (+4.4%) as in the prior estimates (+4%). This increase over the 3-year period includes a decrease of NO_x emissions in 2020 due to COVID-19 lockdowns (**Section 3.4**) and a rebound in 2021. Our posterior estimates indeed show a rebound of NO_x emissions in 2021 compared to 2019 (**Figure 7**)

https://doi.org/10.5194/egusphere-2025-3329
Preprint. Discussion started: 17 July 2025

while the annual mean TROPOMI NO_2 TVCDs decrease over the same period (**Figure A 1**). However, this rebound is not in agreement with H. Li et al. (2024): they estimated an increase of NO_x emissions over China for the first quarter in 2021 compared to 2019 but a decrease of about -3.5% at the annual scale. Appendix A details the sensitivity tests we conducted to assess the effect of meteorological fluctuations from 2019 to 2021 on the observed variations in NO_2 TVCDs between these years. This analysis highlights the large impact of meteorology on the variations of the TVCDs between the two years. Both our inversion framework and that of H. Li et al. (2024) use a CTM to deconvolve this impact from that of the change in emissions when analyzing the variations of the TVCDs. However, CTMs bear relative uncertainties which limit this capability and which are propagated into the emission estimates. The uncertainties in diagnosing emission changes over this period are thus likely high, which may explain the divergent conclusions between the results of H. Li et al. (2024) and our inversion results for 2021.

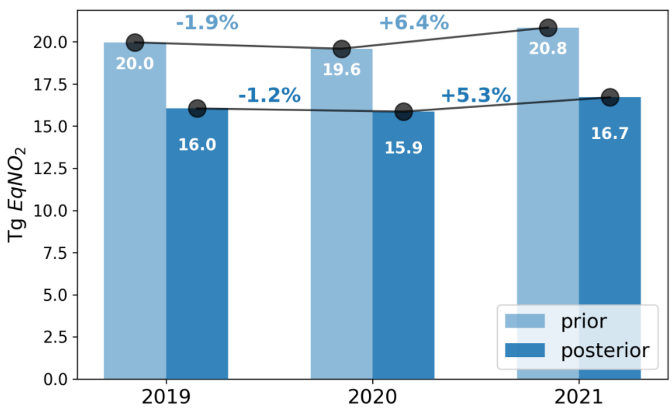

Figure 7. Annual total NO_x emissions (biogenic + anthropogenic) for the period 2019 – 2021, expressed in Tg $EqNO_2$/year for Eastern China in the domain of study. The prior (light blue) and posterior (dark blue) total estimates are shown in white on each bar. The year-on-year changes are shown in percentage above the black lines.

At the scale of the province, the highest increments over the 3-year period are obtained in five main provinces: Liaoning (−49%), Beijing (−38%), Shanghai (−50%), Hubei (−28%), and Guangdong (−18%). There is no correlation between the reduction of prior estimates and the amount of NO_x emitted per province (Figure S9). For instance, although Shanghai emits 471 ktNO_2/year, while Liaoning emits 1398 ktNO_2/year, we find that Shanghai and Liaoning show similar increments of about −50%; in Jiangsu the prior NO_x emissions amount to 1304 ktNO_2/year (similar to Liaoning), while the increment is −25% (compared to an increment of −49% in Liaoning). At the grid-cell resolution, however, the reduction of the prior estimates is highly correlated ($r>0.97$) to the prior estimates. Similar results are found in the study of Plauchu et al. (2024) over France, with strong corrections mainly over dense urban areas. The corrections applied to the prior estimates in Eastern China, on a yearly scale are similar interannually, and they are -66% in 2019 and 2020, and -62% in 2021, per grid box and per year (**Figure 8**).

https://doi.org/10.5194/egusphere-2025-3329
Preprint. Discussion started: 17 July 2025

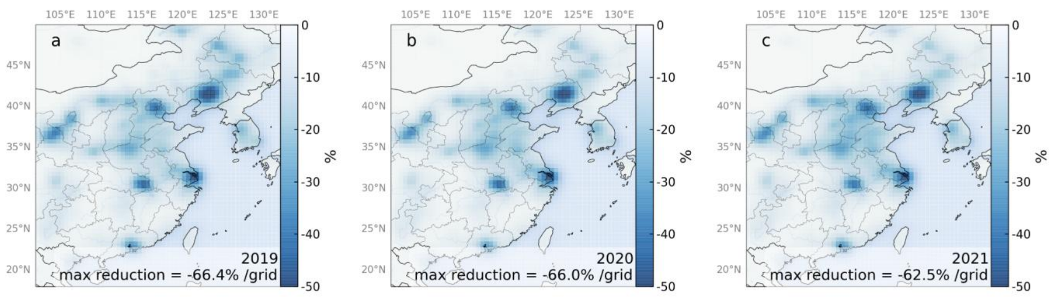

Figure 8. Maps of the yearly increments relative to the prior estimates (%) of annual NO_x emissions at a 0.5° resolution, for the years 2019 to 2021 (a to c).

3.3. Seasonal cycle of NO_x total emissions in Eastern China

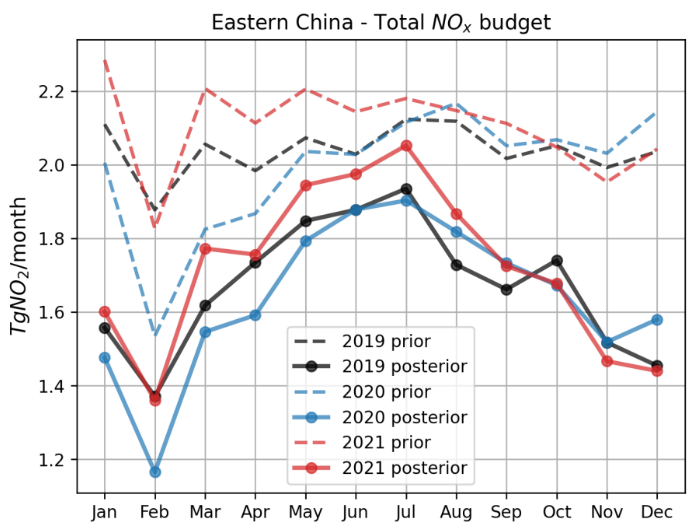

Figure 9. Times series of the monthly prior (in dashed lines) and posterior (in solid lines) total NO_x budget over Eastern China for the years 2019 (black), 2020 (blue) and 2021 (red), expressed in Tg equivalent NO_2 per month.

In contrast with the prior estimate of the emissions (**Section 2.2**), the posterior estimates show an annual maximum systematically occurring in July (**Figure 9**). The peak in summer agrees with the Daily Emissions Constraint by Satellite Observations (DECSO) emissions estimated from inversions assimilating OMI satellite observations (Ding et al., 2015). It suggests that the biogenic emissions may be underestimated in our prior estimates of the NO_x emissions over Eastern China, hence the absence of the peak in the prior estimates during summer; the peak in August 2020 appearing mostly because of the reduction in emissions in winter. This suggestion would be in line with the study of Visser et al. (2019), showing a strong underestimation of the NO_x biogenic emissions from MEGAN in summer over Europe.

https://doi.org/10.5194/egusphere-2025-3329
Preprint. Discussion started: 17 July 2025

Such peaks in summer could also be partly due to anthropogenic emissions, through electricity consumption and the resulting power load, highly correlated with rising temperatures in summer, as shown by Zhang et al. (2009).

In agreement with the prior estimates, the posterior emissions show a minimum in February each year which can be linked to the LNY.

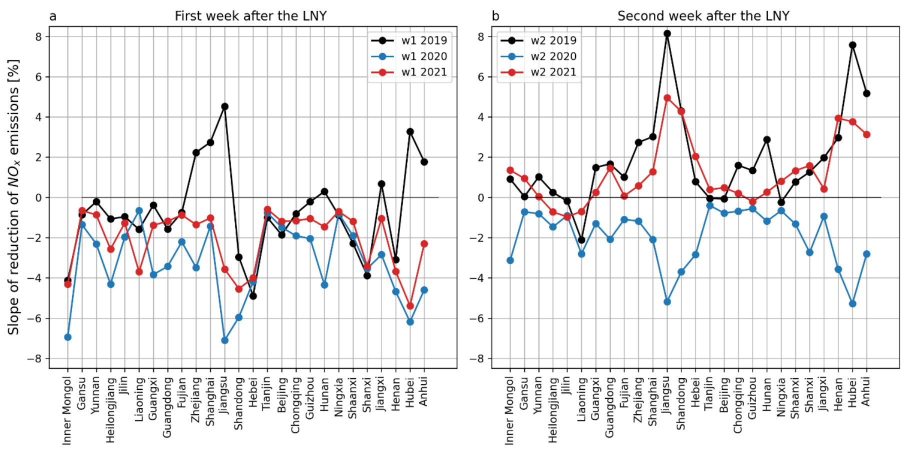

Figure 10. Slope of change in the posterior estimates of NO_x emissions during the first (a) and second (b) weeks following the LNY dates, in 2019, 2020, and 2021 in the Chinese provinces. These slopes of change are calculated for each week separately by computing the slope of a line that connects the first and the last days of the week in question. Week1 of LNY starts on the first day of the New Year, (assigned day1), and week2 starts on day 8. Note that the LNY dates for each year are different; and they fall on 5 February 2019, 25 January 2020, and 12 February 2021.

Our posterior estimates show a consistent relative reduction in NO_x emissions during the first week after LNY in 2019, 2020 and 2021 for 19 out of 26 provinces, by −7% to −0.5% (**Figure 10**). In all provinces, the emissions rebound in the second week during 2019 and 2021, but not in 2020, with reductions between −5.5% and −0.1% (**Figure 10**). We also looked at the 14-day moving means of NO_x emissions in all provinces, but we show only two in **Figure 11**, Henan and Hebei, as both are some of the most densely populated provinces in China (7+ million inhabitants). During the first week following the LNY date, we observe reductions of NO_x emissions, that are around −3.1%, −4.7%, and −3.9% for 2019, 2020 and 2021 respectively in Henan (**Figure 11**a). These reductions are explained by the reduced industrial activities during the LNY holidays. After this decline in emissions, the activity goes back to normal, which is reflected by the rebound in NO_x emissions during the second week following the LNY date in 2019 and 2021 (**Figure 11**). However, in 2020, the reduction is extended to the second week reaching −3.6% in Henan and −2.8% in Hebei, which emphasises the influence of pandemic-related disruptions on NO_x emissions (see **Section 3.4**). Miyazaki et al. (2020) showed that nearly 80% of the emission reductions, during the period 23 Jan – 29 Feb 2020, are due to the lockdown measures in each province. The outdoor restrictions took effect 7 days after the LNY in Henan, falling on 3 February 2020, and 11 days after LNY in Hebei (7 February 2020).

https://doi.org/10.5194/egusphere-2025-3329
Preprint. Discussion started: 17 July 2025

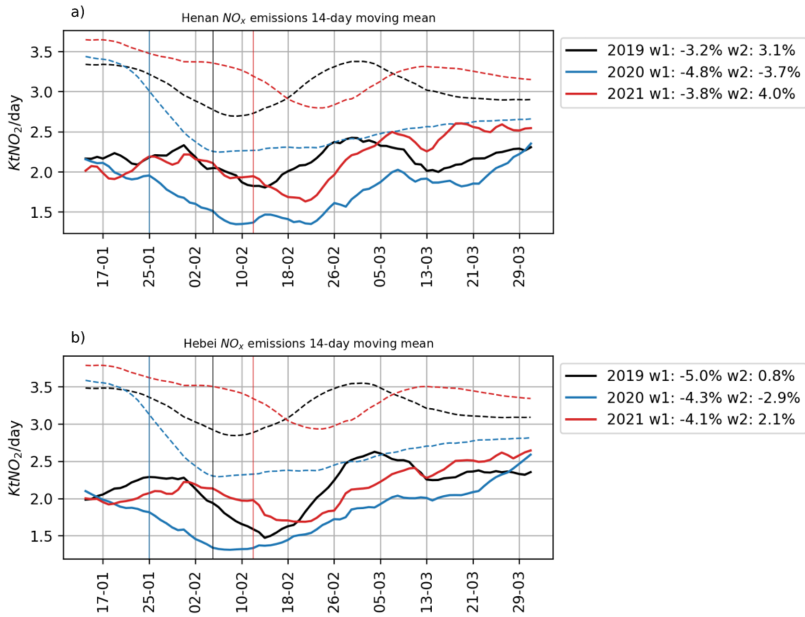

Figure 11. NO_x emissions during the early period of the year, during 2019 (black), 2020 (blue) and 2021 (red). The dotted lines are the prior estimates, and the solid lines are the posterior (corrected) estimates presented as 14-day moving means, for the province of Henan (a) and Hebei (b). In the legend, we show the slope of change during the first (w1) and the second (w2) weeks following the new year date. The Lunar New Year dates are shown as dashed lines in black (for 2019), blue (2020) and red (2021). The slopes of change are calculated on a section of the line (for the posterior estimates). For instance, to get the slopes of week 1, we take the first and last days of the week, we then calculate the slope on a line that connects these two days; it is finally presented as a percentage of change from day 1 to day 7 during the week. The same calculation is applied for week 2, when we take the eighth day after the New Year date, and we count 7 days (day 8 to 14).

3.4. Impact of the COVID-19 lockdowns in Eastern China

Following a usual diagnostic in the literature to assess the change in air pollutant concentrations and emissions due to COVID-19 policies, we characterize the impact of the COVID-19 lockdown in Eastern China in terms of changes in anthropogenic emission estimates from 2019 to 2020 (Fig 12a). While Eastern China total emissions decrease by about −1.8% in 2020 compared to 2019 in CCMM, the posterior emissions show a smaller decrease of about −1.15% (**Figure 7**), less than the one estimated by H. Li et al. (2024) at −2.7% in 2020 compared to 2019.

https://doi.org/10.5194/egusphere-2025-3329
Preprint. Discussion started: 17 July 2025

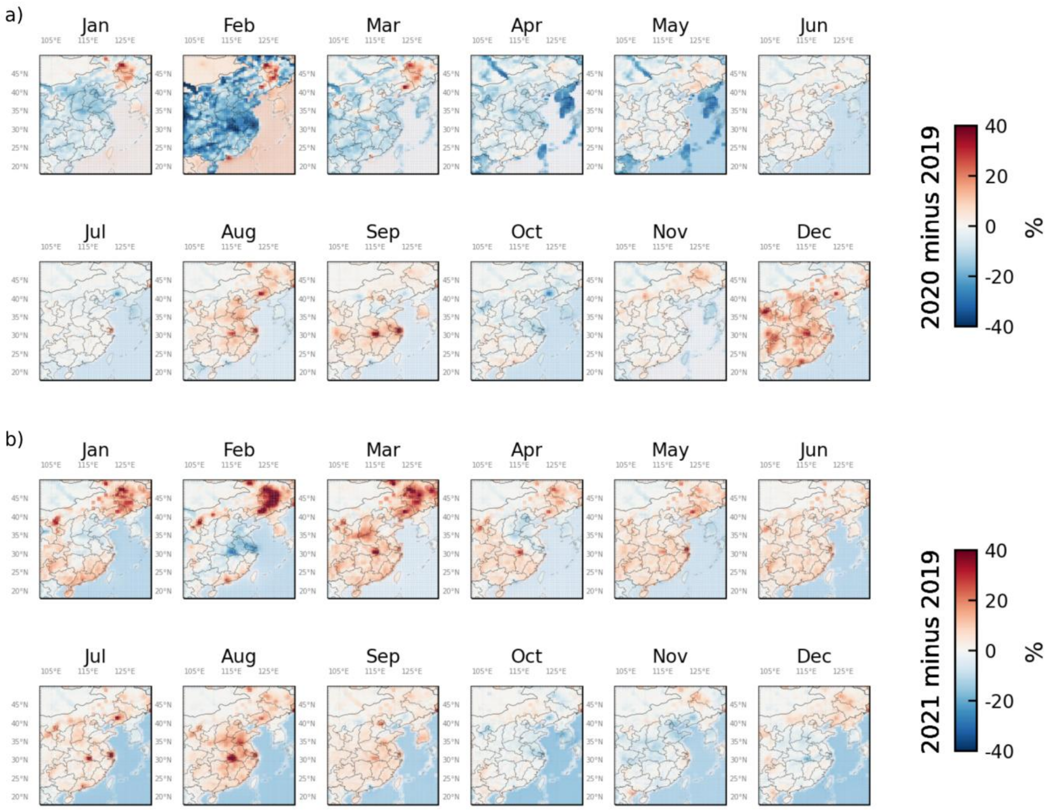

Figure 12. Relative difference (in %) in the posterior estimates of the 0.5° resolution NO_x monthly emission maps during 2020 (a) and 2021 (b) as compared to 2019, over the domain of study. Each plot is the result of the following equation: $\frac{emissions_{year}-emissions_{2019}}{emissions_{2019}} \times 100$, with $emissions_{year}$ being the posterior monthly emissions of the year in question.

February marks the month that witnessed the highest decrease in NO_x emissions: −40% in 2020 compared to 2019. This result agrees with other studies. Zheng et al. (2021) for instance found a decrease of about −36% of the NO_x emissions, leading to a good agreement between NO_2 surface observations and simulations. Miyazaki et al. (2020) found that Chinese NO_x emissions were reduced by −36% from early January to mid-February in 2020 compared to 2019. Finally, Kong et al. (2023) and Stavrakou et al. (2021) also found a decrease of about −40% of the NO_x emissions in February 2020 compared to 2019.

Our configuration allows us to access the spatial distribution of emissions variations. At the provincial resolution, the changes in emissions compared to 2019 are between −3.3% and +3.3% in 2020, and between −1.8% and +11% in 2021 (**Figure 14**). In 2021, all provinces, except Tianjin, show an increase in emissions, most of them between +0.05% and +5.5%; the highest increases are mostly in industrial regions, e.g. Liaoning (+11%), Heilongjiang (+10%), and Jilin (+9.7%).

In February 2020, the reduction of emissions occurred in most of Eastern China (**Figure 12**a). The highest decrease of the NO_x emissions, by more than −30% (±7%), are found in the provinces of

https://doi.org/10.5194/egusphere-2025-3329
Preprint. Discussion started: 17 July 2025

Shanghai, Hubei and Jiangsu (**Figure 13**). On the contrary, emissions increase in the three provinces of Heilongjiang, Jilin and Liaoning located in Northeast China (**Figure 13**). This result agrees with the study of R. Li et al. (2024) also finding an increase in NO_x emissions in these three provinces, due to an increase in industrial production.

During March-April-May of 2020, emissions decreased by −20% along the China-Mongolia-Russia Economic Corridor (**Figure 12**a), one of the main economic belts connecting China through Inner Mongolia, then Mongolia and Russia (World Bank, 2019). This reduction in NO_x emissions may be a result of the decrease in the Chinese exports in April and May 2020 by −15% (GACC, 2020), due to the lock-down measures applied by the Chinese government and to the decrease in Russian exports to China , from ~ $60 billion in 2019 to ~$50 billion in 2020 (GZERO, 2022; OEC, 2022).

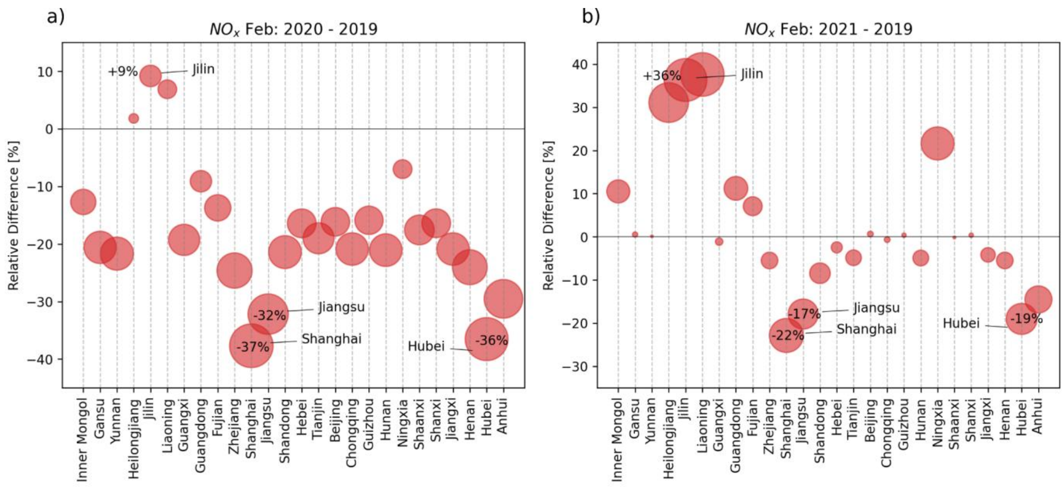

Figure 13. Relative difference in the posterior NO_x emissions during February 2020 (a) and 2021 (b) as compared to 2019, in %, for the provinces illustrated in Figure 1. Note that the scale of the y axes is not the same.

https://doi.org/10.5194/egusphere-2025-3329
Preprint. Discussion started: 17 July 2025

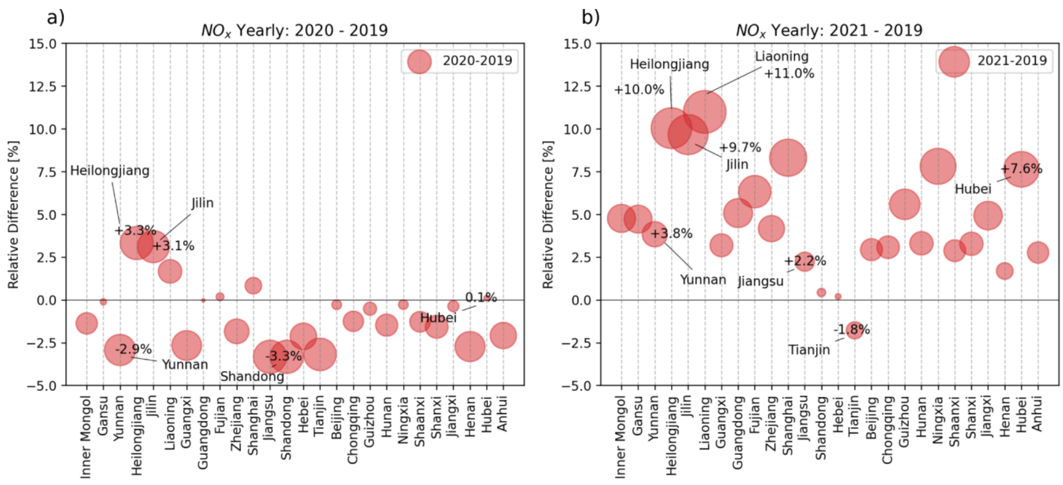

Figure 14. Same as **Figure 13**, but at the annual scale.

4. Conclusions

Monitoring NO_x emissions makes it possible to assess existing air quality policies. In addition to BU approaches (inventories and process-based models), the assimilation of atmospheric data into inverse modelling systems can provide a means for monitoring emissions at a finer time resolution. This study evaluates the potential of satellite data from TROPOMI to provide estimates of NO_x emissions across Eastern China at the monthly and provincial resolutions, using regional-scale atmospheric inversions. For this, TROPOMI NO_2 TVCDs are assimilated in the variational inversion model of the Community Inversion Framework (CIF), coupled to the CHIMERE regional chemistry transport model.

We focused on the changes in Chinese NO_x emissions from 2019 to 2021, with an analysis of the impacts of the Chinese Lunar New Year (LNY) in the three years and of the COVID-19 outbreak in 2020. Each year in 2019, 2020 and 2021, the LNY holidays led to a reduction of emissions during the first week following the New Year day and to an increase of emissions during the second week, except in 2020. Driven by the impact of the LNY combined with the COVID-19 outbreak and the associated lock-down measures, our estimates show a reduction in NO_x emissions of −40% in February 2020 relative to 2019, in Eastern China, in agreement with previous studies. In addition to this, the relatively fine spatial resolution of our framework shows a reduction in emissions along the China-Mongolia-Russia Economic Corridor, of −20% during the spring of 2020, correlated with the measures applied regarding the import–export activities in China. During spring 2020, NO_x emissions decreased in all studied provinces, except three industrial provinces in the North Eastern part of China. At the yearly scale, however, while emissions in 2020 decreased by −1% compared to 2019, we found a rebound of +4% in 2021 compared to 2019.

This study highlights the changes in emissions during the LNY and the COVID-19 periods, and adds a refinement down to the level of provinces. Our regional configuration and inversion model therefore

https://doi.org/10.5194/egusphere-2025-3329
Preprint. Discussion started: 17 July 2025

allow for the estimation of emissions at such a scale, which is crucial for the evaluation of policies at sub-national scales.

Appendix A: Impact of the meteorology on the simulation of NO_2 TVCDs in CHIMERE

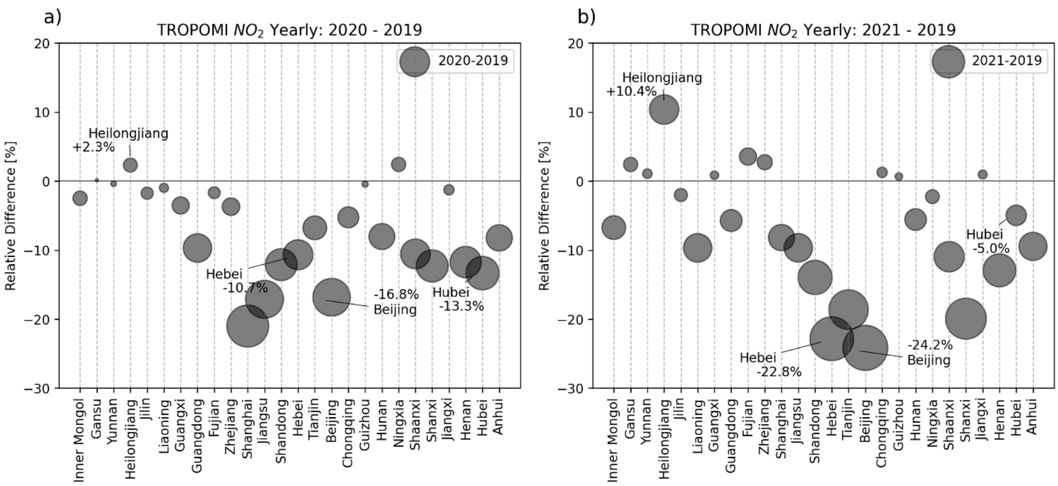

Figure A 1. Relative differences in the NO_2 TROPOMI TVCDs during February 2020 (a) and 2021 (b) as compared to 2019, in %, for the provinces illustrated in **Figure 1**.

Our posterior estimates show a rebound of NO_x emissions in 2021 compared to 2019 (**Figure 7**), with an increase over almost all the provinces (except one) at the annual scale (**Figure 14**b). However, the annual mean TROPOMI NO_2 TVCDs decrease between 2019 and 2021 over most provinces, and, overall, by about −8.3% over Eastern China (**Figure A 1**). These variations in the NO_2 TVCDs are driven by changes in NO_x emissions between 2021 and 2019 but also by fluctuations of the meteorological conditions from 2019 to 2021. In order to understand the relative impact of the meteorology on these variations, we performed a sensitivity test by simulating the NO_2 TVCDs in 2021, using the CCMM inventory for the year 2021 but meteorological fields from the year 2019. This led to increased simulated TVCDs in 2021 by +17% in Eastern China compared to the reference simulation for this year. This change in the simulation of NO_2 TVCDs in 2021 due to using the meteorological forcing from 2019 is shown to be positive throughout the year, but enhanced in January, February, April, and later in November, for Eastern China (**Figure A 2**, a), and Beijing (**Figure A 2**, b), as an illustration of a polluted province.

https://doi.org/10.5194/egusphere-2025-3329
Preprint. Discussion started: 17 July 2025

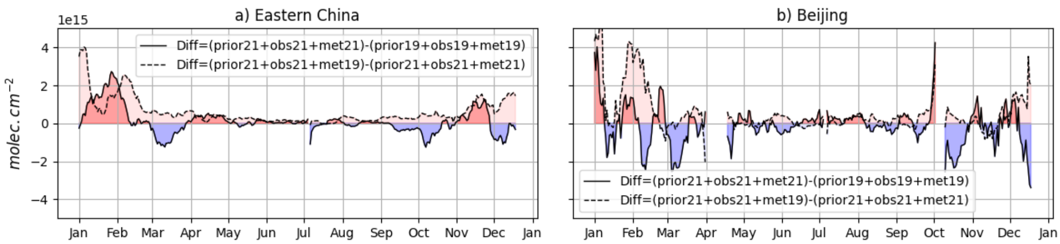

Figure A 2. Time series of the differences between daily 14-day running averages of the NO_2 TVCDs over Eastern China (a) and Beijing (b) from different simulations. The solid lines show the difference between the averages from the reference prior simulations of the TVCDs estimates for 2019 and 2021 (one simulating the TROPOMI observations in 2021 with the meteorological forcing for 2021:prior21+obs21+met21, and the other simulating the data in 2019 with the meteorological forcing for 2019: prior19+obs19+met19). The dotted lines represent the sensitivity to meteorology: they show the difference between the averages from the two simulations of the TROPOMI observations in 2021: the reference prior simulation: prior21+obs21+met21, and the sensitivity test with the meteorological forcing for 2019: prior21+obs21+met19.

While various meteorological factors play a role in the simulation of NO_2 TVCDs, we focus our diagnostics on two parameters: air temperature at an altitude of 2m, and the wind speed at 10m. In Eastern China and at the provincial scale, the two main peaks of sensitivity of the simulated NO_2 TVCDs to the meteorology in January and February, coincide with the positive difference of temperature in January between 2019 and 2021 (**Figure A 2**), and the negative difference of wind speed in February between 2019 and 2021 at both scales (**Figure A 3**a, b). This confirms that the impact of changes in the meteorology on the atmospheric chemistry and transport can explain the decrease of NO_2 concentrations between 2019 and 2021 despite the increase of the NO_x emissions diagnosed from our inversions.

The effect of meteorological variability is thus substantial, and the relative uncertainties in the simulation of such an effect that is inherent in the CTM are propagated into the emission estimates, and thus into the estimate of the variations of these emissions from 2019 to 2021, within the atmospheric inversion frameworks. This likely explains the differences between our results in terms of interannual variability from 2019 to 2021 and those of H. Li et al. (2024), who also used a CTM in their inversion framework, but who reported a decrease in emissions in 2021 relative to 2019.

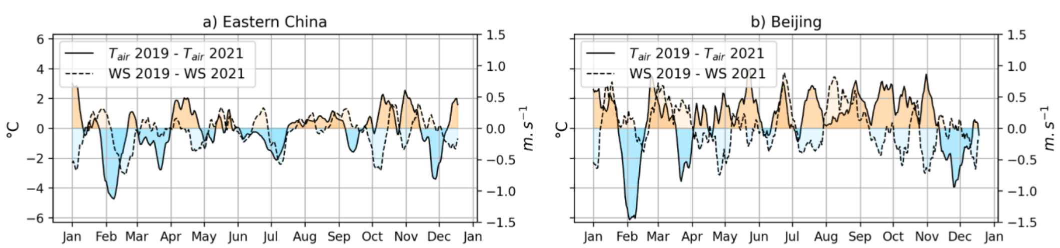

Figure A 3. Time series of the absolute differences of air temperature (at 2m) and wind speed averages, for Eastern China (a) and Beijing (b). All curves represent 14-day running means.

https://doi.org/10.5194/egusphere-2025-3329
Preprint. Discussion started: 17 July 2025

Author contributions

RA, AFC, and GB conceptualized the study and carried out the results analysis. RA carried out the inversions, and the output data analysis, and input data pre-processing. IP, AB, EP developed the CIF inversion system. RP and AFC contributed to the preprocessing for fluxes and satellite observations. BZ provided the CEDS-CarbonMonitor-MEIC (CCMM) inventory used as prior emissions in this study. All the co-authors read the manuscript.

Data availability

TROPOMI-RPRO-v02.04.00 data are freely available through the website https://tropomi.gesdisc.eosdis.nasa.gov/data/S5P_TROPOMI_Level2/S5P_L2__NO2____HiR.2/. The NO_x emissions of this study are available to download through the world-emission platform https://app.world-emission.com/detail/regional/nox/nox. The CEDS-CarbonMonitor-MEIC (CCMM) are available upon a reasonable request from Bo Zheng at bozheng@sz.tsinghua.edu.cn.

Code availability

The CHIMERE code is available here: http://www.lmd.polytechnique.fr/chimere/ (Menut et al., 2013; Mailler et al., 2017). The CIF inversion system (Berchet et al., 2021) is available at https://doi.org/10.5281/zenodo.6304912 (Berchet et al., 2022).

Financial support

A large part of the development and analysis were conducted in the frame of the World Emission project funded by the European Space Agency (ESA). This study has also received funding from the French ANR project ARGONAUT under grant agreement No ANR-19-CE01-0007, from the TOSCA ARGOS project (Centre National d'Etudes Spatiales CNES) and from the French PRIMEQUAL project LOCKAIR under grant agreement No 2162D0010 .

Acknowledgements

We acknowledge the TROPOMI group for the production of the NO_2 retrievals. We wish to thank all the people involved in the preparation, coordination and management of the ESA World Emission project. Finally, we wish to thank Julien Bruna (LSCE) and his team for computer support. We acknowledge the usage of ChatGPT and Perplexity AI to generate bits of python scripts that helped with plotting some of the figures, and for rephrasing certain sentences; in both cases we reviewed and edited the outputs, and no content was used as is.

https://doi.org/10.5194/egusphere-2025-3329
Preprint. Discussion started: 17 July 2025

Competing Interests

The authors declare that they have no conflict of interest.

References

Abdelwahab, M. M., Shalaby, O. A., Semary, H. E., & Abonazel, M. R. (2024). Driving Factors of NOx Emissions in China: Insights from Spatial Regression Analysis. Atmosphere, 15(7), 793. https://doi.org/10.3390/atmos15070793

Agathokleous, E., Feng, Z., Oksanen, E., Sicard, P., Wang, Q., Saitanis, C. J., Araminiene, V., Blande, J. D., Hayes, F., Calatayud, V., Domingos, M., Veresoglou, S. D., Peñuelas, J., Wardle, D. A., De Marco, A., Li, Z., Harmens, H., Yuan, X., Vitale, M., & Paoletti, E. (2020). Ozone affects plant, insect, and soil microbial communities: A threat to terrestrial ecosystems and biodiversity. *Science Advances*, *6*(33), eabc1176. https://doi.org/10.1126/sciadv.abc1176

Atkinson, R. (2000). Atmospheric chemistry of VOCs and NOx. *Atmospheric Environment*, *34*(12), 2063–2101. https://doi.org/10.1016/S1352-2310(99)00460-4

Bauwens, M., Compernolle, S., Stavrakou, T., Müller, J.-F., van Gent, J., Eskes, H., Levelt, P. F., van der A, R., Veefkind, J. P., Vlietinck, J., Yu, H., & Zehner, C. (2020). Impact of Coronavirus Outbreak on NO2 Pollution Assessed Using TROPOMI and OMI Observations. *Geophysical Research Letters*, *47*(11), e2020GL087978. https://doi.org/10.1029/2020GL087978

Berchet, A., Sollum, E., Thompson, R. L., Pison, I., Thanwerdas, J., Broquet, G., Chevallier, F., Aalto, T., Berchet, A., Bergamaschi, P., Brunner, D., Engelen, R., Fortems-Cheiney, A., Gerbig, C., Groot Zwaaftink, C. D., Haussaire, J.-M., Henne, S., Houweling, S., Karstens, U., … Zhao, Y. (2021). The Community Inversion Framework v1.0: A unified system for atmospheric inversion studies. *Geoscientific Model Development*, *14*(8), 5331–5354. https://doi.org/10.5194/gmd-14-5331-2021

Bo, X., Jia, M., Xue, X., Tang, L., Mi, Z., Wang, S., Cui, W., Chang, X., Ruan, J., Dong, G., Zhou, B., & Davis, S. J. (2021). Effect of strengthened standards on Chinese ironmaking and steelmaking emissions. *Nature Sustainability*, *4*(9), 811–820. https://doi.org/10.1038/s41893-021-00736-0

Bovensmann, H., Burrows, J. P., Buchwitz, M., Frerick, J., Noël, S., Rozanov, V. V., Chance, K. V., & Goede, A. P. H. (1999). SCIAMACHY: Mission Objectives and Measurement Modes. *Journal of the Atmospheric Sciences*, *56*(2), 127–150. https://doi.org/10.1175/1520-0469(1999)056<0127:SMOAMM>2.0.CO;2

Bressler, R. D. (2021). The mortality cost of carbon. *Nature Communications*, *12*(1), 4467. https://doi.org/10.1038/s41467-021-24487-w

Burrows, J. P., Hölzle, E., Goede, A. P. H., Visser, H., & Fricke, W. (1995). SCIAMACHY—scanning imaging absorption spectrometer for atmospheric chartography. *Acta Astronautica*, *35*(7), 445–451. https://doi.org/10.1016/0094-5765(94)00278-T

Burrows, J. P., Weber, M., Buchwitz, M., Rozanov, V., Ladstätter-Weißenmayer, A., Richter, A., DeBeek, R., Hoogen, R., Bramstedt, K., Eichmann, K.-U., Eisinger, M., & Perner, D. (1999). The Global Ozone Monitoring Experiment (GOME): Mission Concept and First Scientific Results. *Journal of the Atmospheric Sciences*, *56*(2), 151–175. https://doi.org/10.1175/1520-0469(1999)056<0151:TGOMEG>2.0.CO;2

Carter, W. P. L. (1990). A detailed mechanism for the gas-phase atmospheric reactions of organic compounds. *Atmospheric Environment. Part A. General Topics*, *24*(3), 481–518. https://doi.org/10.1016/0960-1686(90)90005-8

China Power Team. "Measuring China's Manufacturing Might" China Power. December 17, 2024. Updated December 18, 2024. Accessed May 13, 2025. https://chinapower.csis.org/tracker/china-manufacturing/

Chinazzi, M., Davis, J. T., Ajelli, M., Gioannini, C., Litvinova, M., Merler, S., Pastore y Piontti, A., Mu, K., Rossi, L., Sun, K., Viboud, C., Xiong, X., Yu, H., Halloran, M. E., Longini, I. M., & Vespignani, A. (2020). The effect of travel restrictions on the spread of the 2019 novel coronavirus (COVID-19) outbreak. *Science*, *368*(6489), 395–400. https://doi.org/10.1126/science.aba9757

Crippa, M., Guizzardi, D., Muntean, M., Schaaf, E., Dentener, F., van Aardenne, J. A., Monni, S., Doering, U., Olivier, J. G. J., Pagliari, V., and Janssens-Maenhout, G.: Gridded emissions of air pollutants for the period 1970–2012 within EDGAR v4.3.2, *Earth Syst. Sci. Data*, 10, 1987–2013, https://doi.org/10.5194/essd-10-1987-2018, 2018.

Ciarelli, G., Theobald, M. R., Vivanco, M. G., Beekmann, M., Aas, W., Andersson, C., Bergström, R., Manders-Groot, A., Couvidat, F., Mircea, M., Tsyro, S., Fagerli, H., Mar, K., Raffort, V., Roustan, Y., Pay, M.-T., Schaap, M., Kranenburg, R., Adani, M., Briganti, G., Cappelletti, A., D'Isidoro, M., Cuvelier, C., Cholakian, A., Bessagnet, B., Wind, P., and Colette, A.: Trends of inorganic and organic aerosols and precursor gases in Europe: insights from the EURODELTA multi-model experiment over the 1990–2010 period, Geosci. Model Dev., 12, 4923–4954, https://doi.org/10.5194/gmd-12-4923-2019, 2019.

Chu, B., Zhang, S., Liu, J., Ma, Q., & He, H. (2021). Significant concurrent decrease in PM2.5 and NO2 concentrations in China during COVID-19 epidemic. *Journal of Environmental Sciences*, *99*, 346–353. https://doi.org/10.1016/j.jes.2020.06.031

Cooper, M. J., Martin, R. V., Hammer, M. S., Levelt, P. F., Veefkind, P., Lamsal, L. N., Krotkov, N. A., Brook, J. R., & McLinden, C. A. (2022). Global fine-scale changes in ambient NO2 during COVID-19 lockdowns. *Nature*, *601*(7893), 380–387. https://doi.org/10.1038/s41586-021-04229-0

Derognat, C., Beekmann, M., Baeumle, M., Martin, D., & Schmidt, H. (2003). Effect of biogenic volatile organic compound emissions on tropospheric chemistry during the Atmospheric Pollution Over the Paris Area (ESQUIF) campaign in the Ile-de-France region. *Journal of Geophysical Research: Atmospheres*, *108*(D17). https://doi.org/10.1029/2001JD001421

Ding, J., van der A, R. J., Mijling, B., Levelt, P. F., & Hao, N. (2015). NO_x emission estimates during the 2014 Youth Olympic Games in Nanjing. *Atmospheric Chemistry and Physics*, *15*(16), 9399–9412. https://doi.org/10.5194/acp-15-9399-2015

Ding, J., Miyazaki, K., van der A, R. J., Mijling, B., Kurokawa, J., Cho, S., Janssens-Maenhout, G., Zhang, Q., Liu, F., & Levelt, P. F. (2017). Intercomparison of NO_x emission inventories over East Asia. *Atmospheric Chemistry and Physics*, *17*(16), 10125–10141. https://doi.org/10.5194/acp-17-10125-2017

Ding, J., van der A, R. J., Eskes, H. J., Mijling, B., Stavrakou, T., van Geffen, J. H. G. M., & Veefkind, J. P. (2020). NOx Emissions Reduction and Rebound in China Due to the COVID-19 Crisis. *Geophysical Research Letters*, *47*(19), e2020GL089912. https://doi.org/10.1029/2020GL089912

Donzelli, G., & Suarez-Varela, M. M. (2024). Tropospheric Ozone: A Critical Review of the Literature on Emissions, Exposure, and Health Effects. *Atmosphere*, *15*(7), Article 7. https://doi.org/10.3390/atmos15070779

Eskes, H. J., Velthoven, P. F. J. V., Valks, P. J. M., & Kelder, H. M. (2003). Assimilation of GOME total-ozone satellite observations in a three-dimensional tracer-transport model. *Quarterly Journal of the Royal Meteorological Society*, *129*(590), 1663–1681. https://doi.org/10.1256/qj.02.14

Fengxia, G., Min, B., Yijun, M., Zupei, L., Yawen, L., & Haifeng, S. (2016). Temporal and spatial characteristics of lightning-produced nitrogen oxides in China. *Journal of Atmospheric and Solar-Terrestrial Physics*, *149*, 100–107. https://doi.org/10.1016/j.jastp.2016.10.007

Fortems-Cheiney, A., Broquet, G., Plauchu, R., Potier, E., Berchet, A., Pison, I., Martinez, A., Abeed, R., Dufour, G., Coman, A., Savas, D., Siour, G., Eskes, H., Denier van der Gon, H. A. C., & Dellaert, S. N. C. (2024). Decrease of the European NO_x anthropogenic emissions between 2005 and 2019 as seen from the OMI and TROPOMI NO_2 satellite observations. *EGUsphere*, 1–33. https://doi.org/10.5194/egusphere-2024-3679

Fortems-Cheiney, A., Pison, I., Broquet, G., Dufour, G., Berchet, A., Potier, E., Coman, A., Siour, G., & Costantino, L. (2021). Variational regional inverse modeling of reactive species emissions with PYVAR-CHIMERE-v2019. *Geoscientific Model Development*, *14*(5), 2939–2957. https://doi.org/10.5194/gmd-14-2939-2021

GACC. (2020). *General Administration of Customs of the People's Republic of China—Coverage of Major Imports & Exports*. http://english.customs.gov.cn/

Gao, M., Xing, Z., Vollrath, C. et al. Global observational coverage of onshore oil and gas methane sources with TROPOMI. Sci Rep 13, 16759 (2023). https://doi.org/10.1038/s41598-023-41914-8

Gao, C., Zhang, X., Xiu, A., Tong, Q., Zhao, H., Zhang, S., Yang, G., Zhang, M., and Xie, S.: Intercomparison of multiple two-way coupled meteorology and air quality models (WRF v4.1.1–CMAQ v5.3.1, WRF–Chem v4.1.1, and WRF v3.7.1–CHIMERE v2020r1) in eastern China. (2024) *Geosci. Model Dev.*, 17, 2471–2492, https://doi.org/10.5194/gmd-17-2471-2024, 2024.

van Geffen, J., Eskes, H., Compernolle, S., Pinardi, G., Verhoelst, T., Lambert, J.-C., Sneep, M., Ter Linden, M., Ludewig, A., Boersma, K. F., & Veefkind, J. P. (2022). Sentinel-5P TROPOMI NO_2 retrieval: impact of version v2.2 improvements and comparisons with OMI and ground-based data. *Atmospheric Measurement Techniques*, *15*(7), 2037–2060. https://doi.org/10.5194/amt-15-2037-2022

Gilbert, J. C., & Lemaréchal, C. (1989). Some numerical experiments with variable-storage quasi-Newton algorithms. *Mathematical Programming*, *45*(1), 407–435. https://doi.org/10.1007/BF01589113

Gu, D., Wang, Y., Smeltzer, C., & Boersma, K. F. (2014). Anthropogenic emissions of NOx over China: Reconciling the difference of inverse modeling results using GOME-2 and OMI measurements. (2014). *Journal of Geophysical Research: Atmospheres*, *119*(12), 7732–7740. https://doi.org/10.1002/2014JD021644

Guenther, A., Karl, T., Harley, P., Wiedinmyer, C., Palmer, P. I., & Geron, C. (2006). Estimates of global terrestrial isoprene emissions using MEGAN (Model of Emissions of Gases and Aerosols from Nature). *Atmospheric Chemistry and Physics*, *6*(11), 3181–3210. https://doi.org/10.5194/acp-6-3181-2006

GZERO. (2022). *The Graphic Truth: China-Russia trade ties - GZERO Media*. https://www.gzeromedia.com/the-graphic-truth-china-russia-trade-ties

He, H., Wang, Y., Ma, Q., Ma, J., Chu, B., Ji, D., Tang, G., Liu, C., Zhang, H., & Hao, J. (2014). Mineral dust and NOx promote the conversion of SO2 to sulfate in heavy pollution days. *Scientific Reports*, *4*, 4172. https://doi.org/10.1038/srep04172

He, T.-L., Jones, D. B. A., Miyazaki, K., Bowman, K. W., Jiang, Z., Chen, X., Li, R., Zhang, Y., & Li, K. (2022). Inverse modelling of Chinese NO_x emissions using deep learning: Integrating in situ observations with a satellite-based chemical reanalysis. *Atmospheric Chemistry and Physics*, *22*(21), 14059–14074. https://doi.org/10.5194/acp-22-14059-2022

Herman, J., Cede, A., Spinei, E., Mount, G., Tzortziou, M., & Abuhassan, N. (2009). NO2 column amounts from ground-based Pandora and MFDOAS spectrometers using the direct-sun DOAS technique: Intercomparisons and application to OMI validation. Journal of Geophysical Research: Atmospheres, 114(D13), 2009JD011848. https://doi.org/10.1029/2009JD011848

HKTDC Research. (2022, July 25). *Wuhan (Hubei) city information.* HKTDC Research. https://research.hktdc.com/en/data-and-profiles/mcpc/provinces/hubei/wuhan

Hoesly, R. M., Smith, S. J., Feng, L., Klimont, Z., Janssens-Maenhout, G., Pitkanen, T., Seibert, J. J., Vu, L., Andres, R. J., Bolt, R. M., Bond, T. C., Dawidowski, L., Kholod, N., Kurokawa, J., Li, M., Liu, L., Lu, Z., Moura, M. C. P., O'Rourke, P. R., & Zhang, Q. (2018). Historical (1750–2014) anthropogenic emissions of reactive gases and aerosols from the Community Emissions Data System (CEDS). *Geoscientific Model Development*, *11*(1), 369–408. https://doi.org/10.5194/gmd-11-369-2018

Hoesly, R., O'Rourke, P., Braun, C., Feng, L., Smith, S. J., Pitkanen, T., Seibert, J. J., Vu, L., Presley, M., Bolt, R., Goldstein, B., & Kholod, N. (2019). *Community Emissions Data System* (Version Dec-23-2019) [Computer software]. Zenodo. https://doi.org/10.5281/zenodo.3592073

https://doi.org/10.5194/egusphere-2025-3329
Preprint. Discussion started: 17 July 2025

Lambert, J.C., A. Keppens, S. Compernolle, K.-U. Eichmann, M. de Graaf, D. Hubert, B. Langerock, A. Ludewig, M.K. Sha, T. Verhoelst, T. Wagner, C. Ahn, A. Argyrouli, D. Balis, K.L. Chan, M. Coldewey-Egbers, I. De Smedt, H. Eskes, A.M. Fjæraa, K. Garane, J.F. Gleason, F. Goutail, J. Granville, P. Hedelt, K.-P. Heue, G. Jaross, Q. Kleipool, ML. Koukouli, R. Lutz, M.C Martinez Velarte, K. Michailidis, A. Pseftogkas, S. Nanda, S. Niemeijer, A. Pazmiño, G. Pinardi, A. Richter, N. Rozemeijer, M. Sneep, D. Stein Zweers, N. Theys, G. Tilstra, O. Torres, P. Valks, J. van Geffen, C. Vigouroux, P. Wang, and M. Weber. (2024). *Quarterly Validation Report of the Copernicus Sentinel-5 Precursor Operational Data Products #22: April 2018 – February 2024* (S5P MPC Routine Operations Consolidated Validation Report Series, Issue #22, Version 22.01.00, 203 Pp.). https://mpc-vdaf.tropomi.eu/ProjectDir/reports//pdf/S5P-MPC-IASB-ROCVR-24.00.00_FINAL_signed.pdf

Lambert, J.-C., A. Keppens, S. Compernolle, K.-U. Eichmann, M. de Graaf, D. Hubert, B. Langerock, M.K. Sha, E. van der Plas, T. Verhoelst, T. Wagner, C. Ahn, A. Argyrouli, D. Balis, K.L. Chan, M. Coldewey-Egbers, I. De Smedt, H. Eskes, A.M. Fjæraa, K. Garane, J.F. Gleason, J. Granville, P. Hedelt, K.-P. Heue, G. Jaross, ML. Koukouli, E. Loots, R. Lutz, M.C Martinez Velarte, K. Michailidis, A. Pseftogkas, S. Nanda, S. Niemeijer, A. Pazmiño, G. Pinardi, A. Richter, N. Rozemeijer, M. Sneep, D. Stein Zweers, N. Theys, G. Tilstra, O. Torres, P. Valks, J. van Geffen, C. Vigouroux, P. Wang, and M. Weber. (2025). *Quarterly Validation Report of the Copernicus Sentinel-5 Precursor Operational Data Products #26: April 2018 – February 2025*. S5P MPC Routine Operations Consolidated Validation Report series, Issue #26, Version 26.01.00, 223 pp., 15 March 2025. https://s5p-mpc-vdaf.aeronomie.be/ProjectDir/reports//pdf/S5P-MPC-IASB-ROCVR-26.01.00_FINAL.pdf?utm_source=chatgpt.com

Jena, C., Ghude, S. D., Beig, G., Chate, D. M., Kumar, R., Pfister, G. G., Lal, D. M., Surendran, D. E., Fadnavis, S., & van der A, R. J. (2015). Inter-comparison of different NOX emission inventories and associated variation in simulated surface ozone in Indian region. Atmospheric Environment, 117, 61–73. https://doi.org/10.1016/j.atmosenv.2015.06.057

Ju, Ke, et al. "Causal Effects of Air Pollution on Mental Health among Adults——An Exploration of Susceptible Populations and the Role of Physical Activity Based on a Longitudinal Nationwide Cohort in China." Environmental Research, vol. 217, 2023, p. 114761, https://doi.org/10.1016/j.envres.2022.114761

van Geffen, J. H. G. M., Eskes, H. J., Boersma, K. F., Veefkind, J. P., Sneep, M., Linden, M. ter, Beirle, S., Richter, A., & Sanders, B. (2024). TROPOMI ATBD of the total and tropospheric NO2 data products. https://sentiwiki.copernicus.eu/__attachments/1673595/S5P-KNMI-L2-0005-RP%20-%20Sentinel-5P%20TROPOMI%20ATBD%20NO2%20data%20products%202024%20-%202.8.0.pdf

Kong, L., Tang, X., Zhu, J., Wang, Z., Sun, Y., Fu, P., Gao, M., Wu, H., Lu, M., Wu, Q., Huang, S., Sui, W., Li, J., Pan, X., Wu, L., Akimoto, H., & Carmichael, G. R. (2023). Unbalanced emission reductions of different species and sectors in China during COVID-19 lockdown derived by multi-species surface observation assimilation. *Atmospheric Chemistry and Physics*, *23*(11), 6217–6240. https://doi.org/10.5194/acp-23-6217-2023

https://doi.org/10.5194/egusphere-2025-3329
Preprint. Discussion started: 17 July 2025

Le, T., Wang, Y., Liu, L., Yang, J., Yung, Y. L., Li, G., & Seinfeld, J. H. (2020). Unexpected air pollution with marked emission reductions during the COVID-19 outbreak in China. *Science*, *369*(6504), 702–706. https://doi.org/10.1126/science.abb7431

Levelt, P. F., Joiner, J., Tamminen, J., Veefkind, J. P., Bhartia, P. K., Stein Zweers, D. C., Duncan, B. N., Streets, D. G., Eskes, H., van der A, R., McLinden, C., Fioletov, V., Carn, S., de Laat, J., DeLand, M., Marchenko, S., McPeters, R., Ziemke, J., Fu, D., … Wargan, K. (2018). The Ozone Monitoring Instrument: Overview of 14 years in space. *Atmospheric Chemistry and Physics*, *18*(8), 5699–5745. https://doi.org/10.5194/acp-18-5699-2018

Levelt, P. F., Stein Zweers, D. C., Aben, I., Bauwens, M., Borsdorff, T., De Smedt, I., Eskes, H. J., Lerot, C., Loyola, D. G., Romahn, F., Stavrakou, T., Theys, N., Van Roozendael, M., Veefkind, J. P., & Verhoelst, T. (2022). Air quality impacts of COVID-19 lockdown measures detected from space using high spatial resolution observations of multiple trace gases from Sentinel-5P/TROPOMI. *Atmospheric Chemistry and Physics*, *22*(15), Article 15. https://doi.org/10.5194/acp-22-10319-2022

Li, H., Zheng, B., Ciais, P., Boersma, K. F., Riess, T. C. V. W., Martin, R. V., Broquet, G., Van Der A, R., Li, H., Hong, C., Lei, Y., Kong, Y., Zhang, Q., & He, K. (2023). Satellite reveals a steep decline in China's CO2 emissions in early 2022. Science Advances, 9(29), eadg7429. https://doi.org/10.1126/sciadv.adg7429

Li, H., Zheng, B., Lei, Y., Hauglustaine, D., Chen, C., Lin, X., Zhang, Y., Zhang, Q., & He, K. (2024). Trends and drivers of anthropogenic NOx emissions in China since 2020. *Environmental Science and Ecotechnology*, *21*, 100425. https://doi.org/10.1016/j.ese.2024.100425

Li, Q., Guo, F., Ju, X., Liu, Z., Gan, M., Zhang, K., & Cai, B. (2023). Estimation of Lightning-Generated NOx in the Mainland of China Based on Cloud-to-Ground Lightning Location Data. *Advances in Atmospheric Sciences*, *40*(1), 129–143. https://doi.org/10.1007/s00376-022-1329-6

Li, R., Gao, Y., Han, Y., Zhang, Y., Zhang, B., Fu, H., & Wang, G. (2024). Elucidating the mechanisms of rapid O3 increase in North China Plain during COVID-19 lockdown period. *Science of The Total Environment*, *906*, 167622. https://doi.org/10.1016/j.scitotenv.2023.167622

Li, R., Pei, S., Chen, B., Song, Y., Zhang, T., Yang, W., & Shaman, J. (2020). Substantial undocumented infection facilitates the rapid dissemination of novel coronavirus (SARS-CoV-2). *Science (New York, N.Y.)*, *368*(6490), 489–493. https://doi.org/10.1126/science.abb3221

Li, S., Wang, S., Wu, Q., Zhang, Y., Ouyang, D., Zheng, H., Han, L., Qiu, X., Wen, Y., Liu, M., Jiang, Y., Yin, D., Liu, K., Zhao, B., Zhang, S., Wu, Y., & Hao, J. (2023). Emission trends of air pollutants and CO_2 in China from 2005 to 2021. *Earth System Science Data*, *15*(6), 2279–2294. https://doi.org/10.5194/essd-15-2279-2023

Liu, J., Tong, D., Zheng, Y., Cheng, J., Qin, X., Shi, Q., Yan, L., Lei, Y., & Zhang, Q. (2021). Carbon and air pollutant emissions from China's cement industry 1990–2015: Trends, evolution of technologies, and drivers. *Atmospheric Chemistry and Physics*, *21*(3), 1627–1647. https://doi.org/10.5194/acp-21-1627-2021

Liu, Z., Ciais, P., Deng, Z., Davis, S. J., Zheng, B., Wang, Y., Cui, D., Zhu, B., Dou, X., Ke, P., Sun, T., Guo, R., Zhong, H., Boucher, O., Bréon, F.-M., Lu, C., Guo, R., Xue, J., Boucher, E., … Chevallier, F. (2020). Carbon Monitor, a near-real-time daily dataset of global CO2 emission from fossil fuel and cement production. *Scientific Data*, *7*(1), 392. https://doi.org/10.1038/s41597-020-00708-7

Lu, B., Zhang, Z., Jiang, J., Meng, X., Liu, C., Herrmann, H., Chen, J., Xue, L., & Li, X. (2023). Unraveling the O3-NOX-VOCs relationships induced by anomalous ozone in industrial regions during COVID-19 in Shanghai. *Atmospheric Environment (Oxford, England : 1994)*, *308*, 119864. https://doi.org/10.1016/j.atmosenv.2023.119864

Mailler, S., Menut, L., Khvorostyanov, D., Valari, M., Couvidat, F., Siour, G., Turquety, S., Briant, R., Tuccella, P., Bessagnet, B., Colette, A., Létinois, L., Markakis, K., & Meleux, F. (2017). CHIMERE-2017: From urban to hemispheric chemistry-transport modeling. *Geoscientific Model Development*, *10*(6), 2397–2423. https://doi.org/10.5194/gmd-10-2397-2017

Menut, L., Bessagnet, B., Khvorostyanov, D., Beekmann, M., Blond, N., Colette, A., Coll, I., Curci, G., Foret, G., Hodzic, A., Mailler, S., Meleux, F., Monge, J.-L., Pison, I., Siour, G., Turquety, S., Valari, M., Vautard, R., & Vivanco, M. G. (2013). CHIMERE 2013: A model for regional atmospheric composition modelling. *Geoscientific Model Development*, *6*(4), 981–1028. https://doi.org/10.5194/gmd-6-981-2013

Menut, L., Bessagnet, B., Siour, G., Mailler, S., Pennel, R., & Cholakian, A. (2020). Impact of lockdown measures to combat Covid-19 on air quality over western Europe. Science of The Total Environment, 741, 140426. https://doi.org/10.1016/j.scitotenv.2020.140426

Miyazaki, K., Bowman, K., Sekiya, T., Jiang, Z., Chen, X., Eskes, H., Ru, M., Zhang, Y., & Shindell, D. (2020). Air Quality Response in China Linked to the 2019 Novel Coronavirus (COVID-19) Lockdown. *Geophysical Research Letters*, *47*(19), e2020GL089252. https://doi.org/10.1029/2020GL089252

Miyazaki, K., Eskes, H. J., & Sudo, K. (2012). Global NO_x emission estimates derived from an assimilation of OMI tropospheric NO_2 columns. *Atmospheric Chemistry and Physics*, *12*(5), 2263–2288. https://doi.org/10.5194/acp-12-2263-2012

Munro, R., Lang, R., Klaes, D., Poli, G., Retscher, C., Lindstrot, R., Huckle, R., Lacan, A., Grzegorski, M., Holdak, A., Kokhanovsky, A., Livschitz, J., & Eisinger, M. (2016). The GOME-2 instrument on the Metop series of satellites: Instrument design, calibration, and level 1 data processing – an overview. *Atmospheric Measurement Techniques*, *9*(3), 1279–1301. https://doi.org/10.5194/amt-9-1279-2016

NBSC, N. B. of S. of C. (2023). *China Statistical Yearbook 2023*. https://www.stats.gov.cn/sj/ndsj/2023/indexeh.htm

NPC, N. P. C. (2006). *11th Five-Year Plan (2006-2010) for National Economic and Social Development*. https://policy.asiapacificenergy.org/node/115

OEC. (2022). *World trade historical data*. The Observatory of Economic Complexity. https://oec.world/en/profile/world/wld

https://doi.org/10.5194/egusphere-2025-3329
Preprint. Discussion started: 17 July 2025

Owens, R. G. and Hewson, T.: ECMWF Forecast User Guide, ECMWF, Tech. rep., https://doi.org/10.21957/m1cs7h, 2018.

Pei, Z., Han, G., Ma, X., Su, H., & Gong, W. (2020). Response of major air pollutants to COVID-19 lockdowns in China. *Science of The Total Environment*, *743*, 140879. https://doi.org/10.1016/j.scitotenv.2020.140879

Plauchu, R., Fortems-Cheiney, A., Broquet, G., Pison, I., Berchet, A., Potier, E., Dufour, G., Coman, A., Savas, D., Siour, G., & Eskes, H. (2024). NO_x emissions in France in 2019-2021 as estimated by the high spatial resolution assimilation of TROPOMI NO_2 observations. *EGUsphere*, 1–34. https://doi.org/10.5194/egusphere-2024-103

Qin, K., Lu, L., Liu, J., He, Q., Shi, J., Deng, W., Wang, S., & Cohen, J. B. (2023). Model-free daily inversion of NOx emissions using TROPOMI (MCMFE-NOx) and its uncertainty: Declining regulated emissions and growth of new sources. *Remote Sensing of Environment*, *295*, 113720. https://doi.org/10.1016/j.rse.2023.113720

Savas, D., Dufour, G., Coman, A., Siour, G., Fortems-Cheiney, A., Broquet, G., Pison, I., Berchet, A., & Bessagnet, B. (2023). Anthropogenic NOx Emission Estimations over East China for 2015 and 2019 Using OMI Satellite Observations and the New Inverse Modeling System CIF-CHIMERE. *Atmosphere*, *14*(1), Article 1. https://doi.org/10.3390/atmos14010154

Seinfeld, J. H., & Pandis, S. N. (2016). *Atmospheric Chemistry and Physics: From Air Pollution to Climate Change, 3rd Edition | Wiley*. https://www.wiley.com/en-hk/Atmospheric+Chemistry+and+Physics%3A+From+Air+Pollution+to+Climate+Change%2C+3rd+Edition-p-9781118947401

Shaw, S., & Van Heyst, B. (2022). An Evaluation of Risk Ratios on Physical and Mental Health Correlations due to Increases in Ambient Nitrogen Oxide (NOx) Concentrations. *Atmosphere*, *13*(6), Article 6. https://doi.org/10.3390/atmos13060967

Song, M., Zhao, X., Liu, P., Mu, J., He, G., Zhang, C., Tong, S., Xue, C., Zhao, X., Ge, M., & Mu, Y. (2023). Atmospheric NOx oxidation as major sources for nitrous acid (HONO). *Npj Climate and Atmospheric Science*, *6*(1), 1–8. https://doi.org/10.1038/s41612-023-00357-8

Soni, V., Singh, P., Shree, V., & Goel, V. (2018). Effects of VOCs on Human Health. In N. Sharma, A. K. Agarwal, P. Eastwood, T. Gupta, & A. P. Singh (Eds.), *Air Pollution and Control* (pp. 119–142). Springer. https://doi.org/10.1007/978-981-10-7185-0_8

Szopa, S., Foret, G., Menut, L., and Cozic, A.: Impact of large scale circulation on European summer surface ozone: consequences for modeling, Atmos. Environ., 43, 1189–1195, https://doi.org/10.1016/j.atmosenv.2008.10.039, 2008

Tan, P.-H., Chou, C., Liang, J.-Y., Chou, C. C.-K., & Shiu, C.-J. (2009). Air pollution "holiday effect" resulting from the Chinese New Year. *Atmospheric Environment*, *43*(13), 2114–2124. https://doi.org/10.1016/j.atmosenv.2009.01.037

Tang, L., Xue, X., Qu, J., Mi, Z., Bo, X., Chang, X., Wang, S., Li, S., Cui, W., & Dong, G. (2020). Air pollution emissions from Chinese power plants based on the continuous emission monitoring systems network. *Scientific Data*, *7*(1). Scopus. https://doi.org/10.1038/s41597-020-00665-1

Tilstra, L. G., de Graaf, M., Trees, V. J. H., Litvinov, P., Dubovik, O., & Stammes, P. (2024). A directional surface reflectance climatology determined from TROPOMI observations. *Atmospheric Measurement Techniques*, *17*(7), 2235–2256. https://doi.org/10.5194/amt-17-2235-2024

Veefkind, J. P., Aben, I., McMullan, K., Förster, H., de Vries, J., Otter, G., Claas, J., Eskes, H. J., de Haan, J. F., Kleipool, Q., van Weele, M., Hasekamp, O., Hoogeveen, R., Landgraf, J., Snel, R., Tol, P., Ingmann, P., Voors, R., Kruizinga, B., … Levelt, P. F. (2012). TROPOMI on the ESA Sentinel-5 Precursor: A GMES mission for global observations of the atmospheric composition for climate, air quality and ozone layer applications. *Remote Sensing of Environment*, *120*, 70–83. https://doi.org/10.1016/j.rse.2011.09.027

Visser, A. J., Boersma, K. F., Ganzeveld, L. N., and Krol, M. C.: European NOx emissions in WRF-Chem derived from OMI: impacts on summertime surface ozone, Atmos. Chem. Phys., 19, 11821–11841, https://doi.org/10.5194/acp-19-11821-2019, 2019.

Wang, T., Xue, L., Feng, Z., Dai, J., Zhang, Y., & Tan, Y. (2022). Ground-level ozone pollution in China: A synthesis of recent findings on influencing factors and impacts. *Environmental Research Letters*, *17*(6), 063003. https://doi.org/10.1088/1748-9326/ac69fe

Wei, J., Li, Z., Wang, J., Li, C., Gupta, P., & Cribb, M. (2023). Ground-level gaseous pollutants (NO_2, SO_2, and CO) in China: Daily seamless mapping and spatiotemporal variations. *Atmospheric Chemistry and Physics*, *23*(2), 1511–1532. https://doi.org/10.5194/acp-23-1511-2023

World Bank. (2019). *Belt and Road Economics: Opportunities and Risks of Transport Corridors. World Bank. (2019). Belt and Road Economics: Opportunities and Risks of Transport Corridors.* https://www.worldbank.org/en/topic/regional-integration/publication/belt-and-road-economics-opportunities-and-risks-of-transport-corridors

Yin, L., Du, P., Zhang, M., Liu, M., Xu, T., & Song, Y. (2019). Estimation of emissions from biomass burning in China (2003–2017) based on MODIS fire radiative energy data. *Biogeosciences*, *16*(7), 1629–1640. https://doi.org/10.5194/bg-16-1629-2019

Zhang, R.; Zhang, Y.; Lin, H.; Feng, X.; Fu, T.-M.; Wang, Y. NOx Emission Reduction and Recovery during COVID-19 in East China. Atmosphere 2020, 11, 433. https://doi.org/10.3390/atmos11040433

Zhang, Q., Song, Y., Li, M., & Zheng, B. (2020). Anthropogenic Emissions of SO2, NOx, and NH3 in China. In X. Liu & E. Du (Eds.), *Atmospheric Reactive Nitrogen in China: Emission, Deposition and Environmental Impacts* (pp. 13–40). Springer. https://doi.org/10.1007/978-981-13-8514-8_2

Zheng, B., Tong, D., Li, M., Liu, F., Hong, C., Geng, G., Li, H., Li, X., Peng, L., Qi, J., Yan, L., Zhang, Y., Zhao, H., Zheng, Y., He, K., & Zhang, Q. (2018a). Trends in China's anthropogenic emissions since 2010 as the consequence of clean air actions. *Atmospheric Chemistry and Physics*, *18*(19), 14095–14111. https://doi.org/10.5194/acp-18-14095-2018

https://doi.org/10.5194/egusphere-2025-3329
Preprint. Discussion started: 17 July 2025

Zheng, B., Chevallier, F., Ciais, P., Yin, Y., Deeter, M. N., Worden, H. M., Wang, Y., Zhang, Q., & He, K. (2018b). Rapid decline in carbon monoxide emissions and export from East Asia between years 2005 and 2016. *Environmental Research Letters*, *13*(4), 044007. https://doi.org/10.1088/1748-9326/aab2b3

Zheng, B., Zhang, Q., Geng, G., Chen, C., Shi, Q., Cui, M., Lei, Y., & He, K. (2021). Changes in China's anthropogenic emissions and air quality during the COVID-19 pandemic in 2020. *Earth System Science Data*, *13*(6), 2895–2907. https://doi.org/10.5194/essd-13-2895-2021

Zock, J.-P., Verheij, R., Helbich, M., Volker, B., Spreeuwenberg, P., Strak, M., Janssen, N. A. H., Dijst, M., & Groenewegen, P. (2018). The impact of social capital, land use, air pollution and noise on individual morbidity in Dutch neighbourhoods. *Environment International*, *121*, 453–460. https://doi.org/10.1016/j.envint.2018.09.008